We are grateful for the constructive comments of the two reviewers, which encouraged us to reshape the analysis in our resubmission. Below we address the key critiques of each reviewer separately and, where relevant, describe how we have addressed these critiques in our revised manuscript.

Before responding to the individual comments, however, we wanted to provide a brief overview of the key changes that the manuscript has undergone since the last submission. In the original submission, we derived a physically-based model to compute the drag force on a partially submerged boulder in order to determine the conditions under which it is mobile. Based in part on the reviewer comments, as well as on an informal review by Roman DiBiase, we realized that the boulder mobility analysis was too oversimplified to be useful for the problem at hand. Predicting the mobility of an isolated boulder on a smooth river bed (our first approach) is completely different than predicting the mobility of a boulder that is part of a boulder cascade, which is more typical of landslide deposited boulders. For this reason, we now simply use the Shields criterion to calculate the largest movable grain size in each river, which quickly leads to the conclusion that landslide derived boulders are very infrequently, or perhaps never, mobile in the rivers examined.

This realization, in turn, led us to explore another potential explanation for the clear difference in susceptibility to landslide blocking between the two river systems examined. We now argue that the dramatically different sensitivity of the two locations to landslide blocking is related to differences in channel width relative to typical seasonal displacements of earthflows. A synthesis of seasonal earthflow displacements in the Franciscan Mélange shows that the channel width of the Eel River is ~ 5 times larger than the largest annual seasonal earthflow displacements. In contrast, during wet winters, earthflows are capable of crossing the entire channel width of Arroyo Hondo and Alameda Creek. Synthesis of boulder size distribution data, satellite imagery and hydraulic data suggests that in narrow channels earthflows can cross the channel and deposit channel spanning boulder jams that locally impede coarse sediment transport. In contrast, larger channels are able to flow around the toe of earthflows when they impinge on river channels, thereby preventing blocking. We emphasize that this effect is independent of the examined rivers' capacities to actually mobilize coarse debris.

RC1:

"Flow hydraulics and flow competence: My primary concern with the manuscript is the line of reasoning used to calculate the maximum boulder size that can be transported by the Eel River and Arroyo Hondo."

See comments above. We have discarded the boulder mobility analysis in the revision.

"First, as far as I understand, the analysis relies on hydraulic measurements (flow depths, velocities, and discharges) that were made at USGS gage stations that are 2 km (for Oak Ridge earthflow) and 25 km (Mile 201 slide) downstream of the earthflow deposits. Flow depths,

velocities, and discharges at the gage sites are not the same as those at the earthflow deposits. In particular, flow depth and velocity are both sensitive to changes in bed sediment size and channel width. The presence of coarse sediment (such as that found in the earthflow deposits) tends to reduce flow velocities and increase flow depths (e.g., Rickenmann and Recking, 2011). This phenomenon is particularly concerning for this analysis because it may reduce the tendency for boulders to emerge from the flow, which the manuscript proposes as the primary mechanism to stabilize boulders."

This is a good point. While we have discarded the boulder mobility calculation presented in the first submission, we still perform a Shields stress calculation in the new submission and use it to assess boulder mobility. Hence, it is worth considering how the deposition of landslide debris changes coarse sediment transport capacity. That said, given our results that landslide-derived boulder mobility seems very unlikely in the settings examined here, we decided not to embark on a modeling effort to explore the morphodynamics of boulder cascades associated with landslides. However, we now note explicitly that our coarse sediment mobility calculations (page 9, lines 16-22):

"ignore the possible morphodynamic feedbacks that might result from the deposition of large boulders in a channel. On the one hand, landslide derived boulder deposits are steep relative to points upstream and downstream (Figures 5A, 6A), suggesting that the deposition of landslide debris might lead to conditions more favorable to coarse sediment transport. On the other hand, large boulders exert substantial drag on the flow, which can completely offset increases in coarse sediment transport capacity due to the steeper slopes of boulder cascades (Schneider et al., 2016). For this reason, we simply consider the coarse sediment transport capacity of the river at the gage sites as an index of the river's ability to move coarse landslide-derived debris independent of changes in bed morphology caused by that debris."

"Second, I am not sure that it is necessary to introduce a new, untested calculation for boulder mobility when tested models already exist."

We agree. Again, see comments above.

"Simultaneously accounting for the effect of boulders on sediment mobility and flow resistance (for calculation of flow velocity and depth) is tricky and prone to error, but these difficulties can be circumvented by using a critical dimensionless stream power to calculate flow competence (Parker et al., 2011). This criterion has been shown to be a more reliable predictor of sediment mobility than the critical Shields stress in shallow, rough flows (Parker et al., 2011; Ferguson, 2012; Prancevic and Lamb, 2015), and it only requires information about discharge, width, slope, and grain size, all of which the authors have measured at the earthflow deposits. In a quick calculation, I found that this method predicts that the largest mobile sediment during the bankfull flood is ~20 cm for both sites. I may have missed something, but this would suggest that there is not a large difference in flow competence between the two sites. Moreover, these grain sizes seem much more reasonable to me than 2.4 m and 4.9 m. (Can a 4 m boulder really

be transported by a 2-year flood in the Eel?) This estimate of the mobile size fraction is also consistent with the observation that there are very few boulders larger than 30 cm found in the river outside of earthflow deposits at both sites."

We agree with this sentiment. We now use a Shields stress calculation (Table 1) in the draft, which yields very similar results to the back of the envelope calculation performed by RC1: 22 cm 2-year mobility threshold on the Eel River, 31 cm 2-year mobility threshold on Arroyo Hondo. Because our focus is on the mobility of the river independent of the changes that landslides cause to the river (which is an interesting topic, but beyond the scope of what we are trying to accomplish here), we are comfortable using the Shields-based approach, which is not rooted specifically in modeling boulders. For this reason, and because our results are now comparable to RC1's back of the envelope calculation, we have not changed the approach in the paper to that suggested by RC1.

"Comparison of longitudinal profiles: I do think that the longitudinal profiles (Figs. 5- 7) show different earthflow signatures between the study sites, but I think that the comparison would be more compelling if it were more even. The profile of the Eel River is 3x to 4x longer than the other two profiles but is squeezed into the same plot size, which makes it difficult to compare the topographic imprint of earthflows (which seem to not change substantially in size between the two study areas)."

Actually, together the Arroyo Hondo and Alameda Creek sites represent 19 km of river distance and the Eel River site is 30 km, so they are comparable in size.

"Moreover, the slope measurements on the Eel River were made at a resolution 10x larger than at the other study sites, potentially smoothing over some of the variability in slope. I think it would be more convincing to use the same spacing for slope measurements and to zoom in on a portion of the Eel River profile such that the profile examined a similar length to the others two."

This is a good point. To deal with this problem, we have actually done away completely with measuring channel slope in the new draft. Instead, we linearly detrend the river profiles and then plot the residual topography (Figures 5b,6b,7b). The amplitude of the residual topography provides a nice means of identifying perturbations in the channel long profile induced by landslides that are free of the smoothing issues pointing out by RC1. We describe this in more detail in the methods.

"Boulder supply rate: The manuscript focuses on the relative size distributions of coarse sediment supplied to the river between the two study areas. However, it may also be more important to consider the supply rate of coarse boulders. If boulders are delivered very slowly, then the river can rely on bigger, rarer flood events to remove the boulders. It may be outside of the scope of this paper to consider this effect quantitatively, but it should at least be discussed, especially because the Oak Ridge earthflow seems to be sliding 5x faster than the Mile 201

slide. This could be part of the explanation for why there are more big boulders in the river next to the Oak Ridge earthflow.

Also, if the supply rate is important, it is not only the distribution of coarse sediment delivered by the earthflow that matters, but also the proportion that is coarse sediment. What portion of earthflow-derived material is just fines that is just being easily washed away, and does this proportion vary between the two sites? Again, it may be outside of the scope of this paper to measure this, but a discussion is warranted"

This is a good point. To address this issue in the revision we provided a new analysis in which we compared the volumetric flux per unit river channel width for the Boulder Creek earthflow (the largest earthflow along the Eel River) and for Oak Ridge earthflow. This new section (Page 10, lines 18-34) shows that "although the Boulder Creek earthflow has an order of magnitude larger volumetric flux (~ 15,000 m^3/yr) than Oak Ridge earthflow (1700 m^3/yr), the Eel River has an order of magnitude larger channel width (125 m) than Arroyo Hondo (12 m). Hence, earthflow fluxes per unit channel width at the two sites are nearly identical, ~140 m^3/m for Arroyo Hondo and ~130 m^3/m for the Eel River. Despite this similarity, there is no evidence of blocking in the long profile of the Eel River at the location of the Boulder Creek slide, whereas the channel of Arroyo Hondo is clearly blocked at Oak Ridge (Figure 5). For this reason, we also rule out boulder supply relative to transport capacity as a likely driver of the observed morphological differences on the two rivers."

"Grain size distributions: I had a difficult time understanding how the grain size distri- butions were characterized. Were the original distributions calculated using an area- by-number measurement and then transformed to a grid-by-number (or, equivalently, volume-by-weight) (e.g., following Bunte and Abt, 2001)? I'm just a bit confused about how the immobile fraction is transformed from 10% to 80% and 1% to 20% for the two study sites. Please be explicit about which distributions are being used, and perhaps consider using only the volume-by-weight equivalent to avoid confusion."

In the revision, we no longer include the conversion to volume as this is no longer relevant given the change in our findings regarding boulder mobility.

"*Also, the manuscript argues that the sediment sizes measured from aerial imagery are representative of the distribution of coarse sediment, but this is somewhat inconsistent with the rest of the analysis that argues that meter-scale boulders are at least partially mobile. This means that the deposits may also be winnowed with respect to boulders, and not just sediment finer than 30 cm. In other words, the river has likely moved more of the 1 m boulders than 2 m boulders since the boulders were deposited. This might be a small effect, though, especially if the mobile fraction is actually much finer than what is currently reported in the manuscript."*

As suspected by RC1, our results now show that the material capable of being transported in the two rivers is much smaller than what we indicated in the first draft. Hence, we anticipate that the effect described above is probably not fundamental to our analysis.

RC2:

"1. I agree with the comments by Referee Prancevic, who suggested a different approach for quantifying the threshold for motion. Costa (1983, GSA Bulletin) briefly summarizes how when assessing the motion of the largest particles in a channel, the relative roughness of the bed differs than for transporting the median bedload, etc., and such effects can be further considered in the manuscript."

We believe this issue has now been resolved given the changes that we have implemented in the submission, as described at the start of this document, as well as in our response to RC2:

While we have discarded the boulder mobility calculation presented in the first submission, we still perform a Shields stress calculation in the new submission and use it to assess boulder mobility. Hence, it is worth considering how the deposition of landslide debris changes coarse sediment transport capacity. That said, given our results that landslide-derived boulder mobility seems very unlikely in the settings examined here, we decided not to embark on a modeling effort to explore the morphodynamics of boulder cascades associated with landslides. However, we now note explicitly that our coarse sediment mobility calculations (page 9, lines 16-22):

"ignore the possible morphodynamic feedbacks that might result from the deposition of large boulders in a channel. On the one hand, landslide derived boulder deposits are steep relative to points upstream and downstream (Figures 5A, 6A), suggesting that the deposition of landslide debris might lead to conditions more favorable to coarse sediment transport. On the other hand, large boulders exert substantial drag on the flow, which can completely offset increases in coarse sediment transport capacity due to the steeper slopes of boulder cascades (Schneider et al., 2016). For this reason, we simply consider the coarse sediment transport capacity of the river at the gage sites as an index of the river's ability to move coarse landslide-derived debris independent of changes in bed morphology caused by that debris."

"2. Regarding the mobility of the boulders (e.g., (p. 11, line 24); if the boulders are mobile in a 2-yr recurrence flood, and presumably there have been many such floods (and larger floods) since the boulders were deposited, why are they still spatially co- located with the earthflow toes? It would be useful to provide a broader characterization of the spatial occurrence of boulders at each earthflow. For example, are they only present within the earthflow-influenced reach, or are they also located downstream as would be expected from fluvial transport?"

This is an excellent point. Given the results of our updated mobility calculation, the observation that boulders are clustered at the toes of earthflows and not downstream makes sense. In

response to this comment, in the revision we now argue that “it’s entirely plausible that the entire distribution of boulder sizes delivered by earthflows is immobile once delivered to channels in both locations. This interpretation is supported by the fact that gravel bars downstream of the two reference earthflow sites do not contain boulders, and typically do not contain clasts that are even discernable above the ~ 30 cm resolution of the imagery.”

3. I realize the scope of the manuscript is a case study comparison of the two sites, but it would be useful to further document blocking at small drainage area at other sites, as this is the main conclusion of the manuscript. Given the extensive earthflow observations generated by some of the co-authors for the Eel River watershed, it may be possible to assess blockage as a function of drainage area by either by inspection of available imagery or via measurements of floodplain width where suitable topographic data are available. A plot of the proportion of earthflows that block rivers as a function of drainage area could be informative, for example.

We agree with the sentiment of this comment, but feel that such an undertaking is better suited for a future study. We feel that the strength of this contribution is the detailed comparison of the two sites and prefer not to bring in a more synoptic but less detailed analysis in this paper.

“In the discussion of controls on blocking (p. 11), particle jams are noted as a possible mechanism. It is difficult to discern from figures 13 and 14, but are the boulders actually touching one another? Whether they touch or not seems relevant to the arguments (e.g., force chains).”

We have improved these figures (now 12 and 13), and in particular removed the boxes around each boulder that were present in the first submission. We now hope that it is much easier to see the clusters of boulders in each channel and how they are in fact touching, as is clear in the field.

Editorial comments:

P. 1 Line 17: replace “stream gages” with “stream gage data” P. 1 Line 18 and 20: replace “top” with “largest”

These edits are no longer relevant as the section in question has been re-written.

P. 2 Line 9: year missing from citation (same citation in reference list is also missing co-authors)

Fixed.
P. 3 Line 1: add a few words:. . .exploit “discharge data from” USGS. . .

This edit is no longer relevant as the section in question has been re-written.

P. 3 Line 20 units are not consistent throughout; m/a here but m/yr elsewhere.

Changed to m/yr

P. 5 first paragraph: To be consistent with the rest of the text, keep the order the same, present Arroyo Hondo first, then the Eel River.

This edit is no longer relevant as the section in question has been re-written.

P. 5 Line 20: Combine this sentence with the previous paragraph to avoid a one-sentence paragraph.

Done

P 8 Lines 9 and 13: USGS gage websites/numbers are already given, so this is repetative.

We deleted the redundant reference in the revision.

P. 14 Line 14: extra ")"

Changed

P. 14 Line 18: change "period" to "periodic

This edit is no longer relevant as the section in question has been re-written.

River Channel Width Controls Blocking by Slow-moving Landslides in California's Franciscan Mélange

Noah J. Finnegan[1], Kiara N. Broudy[1], Alexander L. Nereson[1], Joshua J. Roering[2], Alexander L. Handwerger[3], Georgina Bennett[4]

[1]Department of Earth and Planetary Sciences, UC Santa Cruz, Santa Cruz, CA, USA 95064, USA
[2]Department of Earth Sciences, University of Oregon, Eugene, OR, 97403-1272, USA
[3]Jet Propulsion Laboratory, California Institute of Technology, Pasadena, CA 91109, USA
[4]School of Environmental Sciences, University of East Anglia, Norwich, Norfolk, NR4 7TJ, UK

Correspondence to: Noah J. Finnegan (nfinnega@ucsc.edu)

Abstract. To explore the sensitivity of rivers to blocking from landslide debris, we exploit two similar geomorphic settings in California's Franciscan Mélange where slow-moving landslides, often referred to as earthflows, impinge on river channels with drainage areas that differ by a factor of 30. Analysis of valley widths and river long profiles over ~ 19 km of Alameda Creek (185 km^2 drainage area) and Arroyo Hondo (200 km^2 drainage area) in central California shows a very consistent picture in which earthflows that intersect these channels force tens of meters of gravel aggradation for kilometers upstream, leading to apparently long-lived sediment storage and channel burial at these sites. In contrast, over a ~ 30 km section of the Eel River (5547 km^2 drainage area) there are no knickpoints at or aggradation upstream of locations where earthflows impinge on its channel. Hydraulic and hydrologic data from USGS gages on Arroyo Hondo and the Eel River, combined with measured size distributions of boulders input by landslides for both locations, suggests that landslide derived boulders are not mobile at either site during the largest floods (> 2 year recurrence) with field measured flow depths. We therefore argue that boulder transport capacity is an unlikely explanation for the observed difference in sensitivity to landslide inputs. At the same time, we find that earthflow fluxes per unit channel width are nearly identical for Oak Ridge earthflow on Arroyo Hondo, where evidence for blocking is clear, and for the Boulder Creek earthflow on the Eel River, where evidence for blocking is absent. These observations suggest that boulder supply is also an unlikely explanation for the observed morphological differences along the two rivers. Rather, we argue that the dramatically different sensitivity of the two locations to landslide blocking is related to differences in channel width relative to typical seasonal displacements of earthflows. A synthesis of seasonal earthflow displacements in the Franciscan Mélange shows that the channel width of the Eel River is ~ 5 times larger than the largest annual seasonal displacement. In contrast, during wet winters, earthflows are capable of crossing the entire channel width of Arroyo Hondo and Alameda Creek. In support of this interpretation, satellite imagery shows that immobile earthflow-derived boulders are generally confined to the edges of the channel on the Eel River. By contrast, immobile earthflow-derived boulders jam the entire channel on Arroyo Hondo. Our results imply that the narrow, lower drainage area, upper portions of earthflow-dominated catchments may be particularly prone to blocking. By

Deleted: Fluvial boulder transport controls valley blocking by earthflows in the California Coast Range, USA.¶

Deleted: At

Deleted: sites

Deleted: (Arroyo Hondo, central California and the Eel River, northern California), earthflowswhere slow-moving landslides, often

Deleted: We compare these sites to explore how river flow depth, width, and velocity control river resilience to valley blocking and aggradation that occurs as earthflows deliver large quantities of coarse sediment to the channel network. We measure the…

Deleted: distribution of earthflow-

Deleted: (>30 cm) delivered to each channel and use USGS stream gages to quantify the are

Deleted: fraction of boulders for a

Deleted: -

Deleted: interval flood. For Arroyo Hondo, only the top ~10% of boulders are immobile (> 2.4 m diameter), however, this portion of the distribution represents ~80% of the volume of coarse,) with field

Deleted: -derived material. For

Deleted: top ~1% of boulders are immobile (> 4.9 m diameter), a fraction that represents only ~20% by volume. Satelliteobserved

Deleted: boulders in Arroyo Hondo jam the entire channel and coincide with knickpoints and aggradation for km's upstream. By comparison, immobile boulders in the Eel River are sparsely distributed and earthflow-derived boulders are

Deleted: . Moreover, the Eel River valley and long profile show little evidence of perturbation despite numerous well documented active earthflows along its length. This contrast suggests valley blocking is very sensitive to the mobility of the coarsest fraction of sediment. In this way, earthflow-impacted channels may act like step-pool channels, where channel-spanning boulder jams locally impede coarse sediment transport. In support of this view, the ratio of channel width to the threshold diameter for immobile boulders on Arroyo Hondo is ~5 (as opposed to ~25 for the Eel River), suggesting the river is susceptible to jamming. on the Eel River

Deleted: Valley blocking, in turn, may inhibit

inhibiting the upstream propagation of base-level signals, valley blocking earthflows may therefore promote the formation of so-called "relict topography."

Introduction

River incision into bedrock drives landscape change in unglaciated settings and is the key process linking tectonics and topography (Whipple, 2004). However, the process of river incision is sensitive to the amount and caliber of coarse sediment supplied from hillslopes (Sklar and Dietrich, 2001, 2004) such that coarse sediment input can accelerate (Cook et al., 2013) or arrest incision (Bull, 1990). This non-linearity reflects the dual role of coarse sediment in providing abrasive tools and inhibiting incision when deposited on the bed (Gilbert, 1877).

The dependence of river incision on hillslope-derived coarse sediment input also means that river incision, which provides the lower boundary condition for hillslopes, and landsliding, which delivers coarse sediment to channels, are coupled (Golly et al., 2017; Ouimet et al., 2007; Schuerch et al., 2006). The apparent strength of this coupling, however, varies widely. On the one hand, river aggradation and valley blockages triggered by rock falls and rock avalanches can persist for timescales as long as 10^4 years (Korup et al., 2006). Similarly, elevated coarse sediment loads following co-seismic landslides can attenuate over timescales as long as centuries (Stolle et al., 2019; Yanites et al., 2010). These examples suggest that landsliding provides a strong negative feedback on river incision by causing long lived burial events and hence hiatuses in downcutting (Miller et al., 2016; Ouimet et al., 2007; Yanites et al., 2010). These examples also suggest that valley aggradation or incision following a landslide may occur long after evidence for the landslide itself is recognizable in the landscape. On the other hand, in some settings little evidence of valley blocking is seen despite extremely high rates of landsliding (Korup et al., 2010), suggesting a contrasting view in which rivers are not strongly perturbed following landslides and in which landsliding occurs essentially passively in response to river incision (Burbank et al., 1996; Larsen and Montgomery, 2012).

Work devoted to the problem of landslide dam formation from the perspective of landslide processes emphasizes both the rates of material delivery to channels as well as the width of river valleys into which debris is delivered as key controls on dam formation (Costa and Schuster, 1988; Korup, 2002). That said, comparatively less work has focused on fluvial controls on the resilience of rivers to landslide inputs. With this in mind, here we explore what governs river resilience to valley blocking by landslide debris. Towards this end, we exploit two similar geomorphic settings in the California Coast Range where slow-moving landslides, often referred to as earthflows, impinge on river channels with drainage areas that differ by a factor of 30. By comparing mapped landslide locations to long profile and valley morphology, we establish locations where valley blocking from earthflows has occurred at each site. We then explore factors that govern apparent contrasts in river resilience to valley blocking in otherwise similar geomorphic and geologic settings.

Deleted: and

Deleted: and fluvial hanging valleys.

Deleted: River incision into bedrock drives landscape change in unglaciated settings and is the key process linking tectonics and topography (Whipple, 2004). However, the process of river incision is sensitive to the amount and caliber of sediment supplied from hillslopes (Sklar and Dietrich, 2001, 2004) such that coarse sediment input can accelerate (Cook et al., 2013) or arrest incision (Scherler et al., 2016). This non-linearity reflects the dual role of coarse sediment in providing abrasive tools and inhibiting incision when deposited on the bed (Gilbert, 1877). ¶

¶

The dependence of river incision on hillslope sediment input also means that river incision, which provides the lower boundary condition for hillslopes, and landsliding, which delivers coarse sediment to channels, are coupled (Golly et al., 2017; Ouimet et al., 2007). The apparent strength of this coupling, however, varies widely. On the one hand, river aggradation and valley blockages triggered by rock falls and rock avalanches can persist for timescales as long as 10^4 years (Korup et al., 2006). Similarly, elevated sediment loads following co-seismic landslides can attenuate over timescales as long as centuries (Stolle et al.). These examples suggest that landsliding provides a strong negative feedback on river incision by causing long lived burial events and hence hiatuses in downcutting (Bennett et al., 2016a; Ouimet et al., 2007). These examples also suggest that valley aggradation or incision following a landslide may occur long after evidence for the landslide itself is recognizable in the landscape. On the other hand, in some settings little evidence of valley blockage is seen despite extremely high rates of landsliding (Korup et al., 2010). In addition, elevated sediment loads following co-seismic landslides can relax in as little as a few years (Hovius et al., 2011). These examples suggest a contrasting view in which rivers are not strongly perturbed following landslides and in which landsliding occurs essentially passively in response to river incision (Burbank et al., 1996; Larsen and Montgomery, 2012).¶

¶

There are at least two important factors that govern the sensitivity of rivers to landslide inputs. First, the type and size of landslide dictates the rate and amount of material delivered to channels. This is likely why landslide dam formation is more common following debris and rock avalanches, which can deliver large volumes of sediment rapidly to rivers (Costa and Schuster, 1988). In addition, valley width is a clear control on landslide dam formation because, all else being equal, a narrow valley can be more easily blocked (Costa and Schuster, 1988). Second, the capacity of a river to transport coarse debris buffers rivers against the effects of landslide inputs. Notably, the study of Larsen and Montgomery (2012) documented landslide rates along the Yarlung Tsangpo River, the most powerful river in the Himalaya (Finlayson et al., 2002), and found that this location lacks evidence for landslide dams (although evidence for valley blocking moraines is plentiful here) despite extremely high erosion rates (Korup et al., 2010).¶

¶

While considerable work has been devoted to the problem of landslide dam formation from the perspective of landslide processes (Costa and Schuster, 1988; Korup, 2002), comparatively less work has focused on fluvial controls on the resilience of rivers to landslide inputs. Accordingly, here we explore what governs river resilience to valley blocking by landslide debris. Towards this end, we exploit two similar geomorphic settings in the California Coast Range where slow-moving landslides, often referred to as earthflows, ... [1]

In this paper we consciously use the term valley blocking instead of damming. While valley blocking from earthflows, like damming, can cause aggradation for kilometers upstream, to depths of several 10's of meters, it is unusual that earthflows deposit sediment rapidly enough to cause the formation of lakes. Hence, to avoid confusion, here we adopt the term valley blocking.

1 Geologic and Geomorphic Setting

The Franciscan Complex is an assemblage of variably deformed and metamorphosed rock units formed in a subduction zone during the Mesozoic and early Cenozoic eras (Wakabayashi, 1992). With widespread occurrence throughout the state of California (Fig. 1), Franciscan lithologies include primarily detrital sedimentary rocks such as sandstones and argillaceous mélanges that are well known for their low strength and high susceptibility to slope failure. Many documented instances of earthflows, in particular, in California occur within these units (Iverson and Major, 1987; Keefer and Johnson, 1983; Kelsey, 1978; Roering et al., 2015; Scheingross et al., 2013). Earthflows are characterized by a flow-like appearance and persistence over decades to centuries (Hungr et al., 2014). They form above fine-grained bedrock in plastic, clayey soil and are commonly large (>500 m long) and deep (>5 m). They typically move at rates less than ~10 m/yr (Baum et al., 2003), however they can also display more rapid, but short-lived surge-like events approaching ~m/d (Hungr et al., 2014). Active earthflows frequently extend from ridge-tops to valley-bottoms (Mackey and Roering, 2011) and are classically described as having an 'hourglass' planform outline, with a bowl-shaped source area, an elongate transport zone, and a lobate toe (Keefer and Johnson, 1983). Notwithstanding their name and appearance, most earthflow movement occurs by sliding along discrete basal and lateral shear surfaces (Fleming and Johnson, 1989; Keefer and Johnson, 1983; Simoni et al., 2013; Vulliet and Hutter, 1988; Zhang et al., 1991). In this paper, we exploit two locations in the California Coast Ranges where earthflows impinge on channels of greatly differing scale. Both of these locations are underlain by the Franciscan Complex lithologic units. Below we describe each location separately.

1.1 Arroyo Hondo and Alameda Creek

Arroyo Hondo (200 km^2) and upper Alameda Creek (185 km^2) drain a rugged region of the northern Diablo Range, northeast of San Jose, California (Fig. 1 and Fig. 2). Their confluence occurs just downstream of Calaveras Dam, which impounds Calaveras Reservoir, the largest reservoir in the San Francisco Bay Area. Where each creek crosses the actively uplifting Diablo Range, it has incised a deep (~ 600 m) canyon into Franciscan formation sandstone and mudstone mélange. The walls of these canyons are draped with earthflows (Fig. 2 and Fig. 3). One of them, Oak Ridge earthflow, was studied by Nereson and Finnegan (2019), who analyzed its historical motion from air photos that span 1937-2017. Within the persistently active ~ 100 m wide transport zone of the earthflow, the mean velocity was ~ 2.15 m/yr over this time interval (Nereson and Finnegan, 2019). We use field observations and detailed measurements of boulder size distributions at Oak Ridge earthflow as a reference site from which we make more generalized inferences about the relationship between earthflows and valley blocking in Alameda Creek and Arroyo Hondo. Here we analyze approximately 11 km of Alameda

Deleted: The Franciscan Complex is an assemblage of variably deformed and metamorphosed rock units formed in a subduction zone during the Mesozoic and early Cenozoic eras (Wakabayashi, 1992). With widespread occurrence throughout the state of California (Figure 1), Franciscan lithologies include primarily detrital sedimentary rocks such as sandstones and argillaceous mélanges that are well known for their low strength and high susceptibility to slope failure. Many documented instances of earthflows, in particular, in California occur within these units (Iverson and Major, 1987; Keefer and Johnson, 1983; Kelsey, 1978; Roering et al., 2015; Scheingross et al., 2013). Earthflows are characterized by a flow-like appearance and persistence over decades to centuries (Hungr et al., 2014). They form above fine-grained bedrock in plastic, clayey soil and are commonly large (>500 m long), deep (>5 m), and move at rates less than ~10 m/a (Baum et al., 2003). Active earthflows frequently extend from ridge-tops to valley-bottoms (Mackey and Roering, 2011) and are classically described as having an 'hourglass' planform outline, with a bowl-shaped source area, an elongate transport zone, and a lobate toe (Keefer and Johnson, 1983). Notwithstanding their name and appearance, most earthflow movement occurs by sliding along discrete basal and lateral shear surfaces (Fleming and Johnson, 1989; Keefer and Johnson, 1983; Simoni et al., 2013; Vulliet and Hutter, 1988; Zhang et al., 1991). In this paper, we exploit two locations in the California Coast Ranges where earthflows impinge on channels of greatly differing scale. Both of these locations are underlain by the Franciscan Complex lithologic units. Below we describe each location separately.¶

¶

1.1 Arroyo Hondo and Alameda Creek ¶

Arroyo Hondo (200 km^2) and upper Alameda Creek (185 km^2) drain a rugged region of the northern Diablo Range, northeast of San Jose, California (Figure 1, 2).…

Deleted: Figures 2, 3). One of them, Oak Ridge earthflow, was studied by Nereson and Finnegan (2018), who analyzed its historical motion from air photos that span 1937-2017. Although sliding velocity for the earthflow varied both temporally and spatially, within the persistently active ~ 100 m wide transport zone of the earthflow the mean velocity was 2.15 m/yr Nereson and Finnegan (2018).…

Deleted: 20

Creek and 8 km of Arroyo Hondo. These are reaches where the authors have performed extensive field reconnaissance. A USGS gage on Arroyo Hondo is located within the study section considered here (https://waterdata.usgs.gov/usa/nwis/uv?11173200) (Fig. 2). At this location, Arroyo Hondo has a drainage area of 200 km^2. Annual rainfall at Oak Ridge earthflow is 53 cm, most of which occurs between October and May (Nereson and Finnegan, 2019)

1.2 Eel River

We also exploit a study site developed by Mackey and Roering (2011) along a ~ 30 km section of the main stem Eel River between Dos Rios and Alderpoint (Fig. 1, and Fig. 4) in the northern California Coast Range in Mendocino, Humboldt, and Trinity counties. At this location, the Eel River cuts an ~ 800 m deep canyon into actively uplifting rocks of the Central Belt of the Franciscan Complex (McLaughlin et al., 2000). The Central Belt consists of mudstone mélange, similar to Arroyo Hondo and Alameda Creek, that surrounds coherent blocks of various lithologies that can be as large as entire mountains (Roering et al., 2015). At this location, Mackey and Roering (2011) tracked the historical motion of 122 earthflows from 1944 to 2006. Over this period, the median annual sliding velocity of all landslides was 0.4 m/yr. More recent work (Bennett et al., 2016b) revealed a significant deceleration of these earthflows during the historic California drought from 2012-2015, and both recent acceleration and activation of new slides during the extremely wet winter of 2016-2017 (Handwerger et al., 2018, 2019). We analyze river data from a USGS gage located at Fort Seward (https://waterdata.usgs.gov/ca/nwis/uv?site_no=11475000), approximately 12 km downstream of Alderpoint. At this location, the Eel River has a drainage area of 5547 km^2. Because there are no major tributary junctions between the study reach and the Fort Seward Gage, we assume the Fort Seward gage is approximately representative of the conditions within the study section. Annual rainfall at Alderpoint is 130 cm (Mackey and Roering, 2011). We use a reference site at an active earthflow, referred to as the "Mile 201" slide by Mackey and Roering (2011), just downstream from the confluence of Kekawaka Creek with the Eel River (Fig. 4). At this location, we make detailed measurements of boulder size distributions being supplied to the Eel River by earthflows via high resolution aerial imagery.

2 Methods

2.1 Landslide Impacts on Channels

We use river long profile morphology (along with floodplain width, described below) to assess the fluvial response to earthflow inputs. Earthflow deposits are commonly comprised of large boulders, leading to steep boulder cascades downstream of landslide blockages, which in turn drive fluvial aggradation upstream (Kelsey, 1978). Thus the topographic signature of valley blocking landslides in river long profiles is an anomalously low gradient reach, representing the upstream aggradational section, that grades downstream to the lip of a steep knickpoint, which represents the valley blocking deposit (Ouimet et al., 2007). To highlight such reaches, we linearly detrend the river long profiles for each of the three reaches examined (Fig. 5b, Fig. 6b, and Fig. 7b). The residual topography following detrending highlights locations where the

Deleted: 10

Deleted: Figure

Deleted: (Nereson and Finnegan, 2018).

Deleted: Figure

Deleted: ,

Deleted: and

Deleted: a

Deleted: (McLaughlin et al., 2000).

Deleted: has revealed a significant deceleration of these earthflows during the historic California drought from 2012-2015.revealed a

Deleted: 2001),

Deleted: Figure

Deleted: We use measurements of local channel slope (along with floodplain width, described below) to assess the fluvial response to earthflow inputs. Earthflow deposits are commonly comprised of large boulders, leading to steep boulder cascades downstream of landslide blockages, which in turn drive fluvial aggradation upstream (Kelsey, 1978). To highlight such reaches, we calculate river bed slope over a length-scale that is comparable to the backwater length-scale (~ flow depth/ bed slope) (Paola and Mohrig, 1996; Pfeiffer and Finnegan, 2017). For the Eel River site (as described in more detail later) we use the flow depth calculated for a 2-year recurrence interval flood, 7.1 m, combined with the mean bed slope over the 30 km reach, 0.0026, to calculate a backwater length of ~2700 m. For the Arroyo Hondo site, we use the flow depth calculated for a 2-year recurrence interval flood, 1.6 m, combined with the mean bed slope over the 30 km reach, 0.016, to calculate a backwater length of ~100 m. Because Alameda Creek has a similar drainage area to Arroyo Hondo at our study location, we calculate slope over a similar length-scale for Alameda Creek. By using the backwater length to calculate slope, our measurements of slope are relatively insensitive to perturbations in river elevation that are smaller than the flow depth, such as those arising, for example, from pool riffle sequences. ¶
¶

channel departs from a smoothly graded profile. In addition, the amplitude of the residual topography provides a direct measurement of the height of valley blockages and hence the depth of fluvial aggradation upstream of blockages.

Valley aggradation in a steep-walled canyon leads naturally to floodplain widening simply by virtue of the triangular cross-section of a valley (Mey et al., 2015; Reneau and Dietrich, 1991). For this reason, we also make measurements of local floodplain width to complement our channel slope measurements. The logic here is that deep aggradation upstream of landslide blockages should be reflected in local floodplain width. We use LiDAR-derived slope maps to help identify the slope break that marks the intersection of the steep canyon wall with the low gradient valley bottom alluvial deposits. We hand digitized a line corresponding to this slope break along each side of the three canyon reaches examined here. We then rasterized this line and used ArcGIS to calculate the Euclidean distance from both the right and left edges of the floodplain. The sum of these Euclidean distance maps within the active floodplain yields an approximation of the local floodplain width, which we extract at each point where we measure elevation. To highlight potentially landslide impacted river reaches we look for points that mark rapid changes in valley width (from wide to narrow) and rapid changes in river slope (from low to high).

For both sites, we take advantage of LiDAR-derived topography data to make measurements of river channel morphology. For the Eel site, we use LiDAR data as described by Mackey and Roering (2011). For the Alameda Creek/Arroyo Hondo site, we use 1/9 second USGS NED data. We hand digitized thalweg profiles for both study locations using shaded relief maps. We extracted elevation points every 100 m for the Eel River and every 10 m for the Arroyo Hondo and Alameda Creek sites. This difference in spacing reflects the approximate difference in channel width for the two locations.

2.2 Quantification of Boulder Size Distributions

We use Google Earth imagery, which we exported to ArcGIS after re-georeferencing, to map boulder size distributions entering channels at the toes of active earthflows at our two reference sites. The toe of Oak Ridge Earthflow is currently collapsing along a series of rotational failures into Arroyo Hondo (Nereson and Finnegan, 2019), which in combination with pre-historic motion of the earthflow toe, has resulted in an accumulation of large, unsorted earthflow-derived boulders in the channel of Arroyo Hondo at the base of the earthflow. We digitized all visible boulders (n = 329) as ellipses, which we then fit with rectangles to quantify the major and minor axis lengths of the boulders. The imagery enable us to identify boulders down to 30 cm in diameter. Because of the proximity of boulders to the earthflow toe and the absence of sorting in the field, we treat the distribution of boulders at the toe of Oak Ridge earthflow as representative of the coarse fraction of material (larger than the 30 cm detection limit) that is eroding out of the earthflow once its fine matrix has been winnowed away (e.g., Kelsey, 1978). This interpretation is supported by the fact that it is impossible to differentiate individual grains on bar surfaces upstream of the earthflow toe in aerial imagery. In other words, the bulk of the distribution of bedload that is moved by the river appears to fall below the detection limit in the aerial imagery.

Deleted: (Mey et al., 2015; Reneau and Dietrich, 1991).

Deleted: euclidean

Deleted: euclidean

Deleted: ¶
¶

Deleted:) (e.g., Ouimet et al., 2007).

Deleted: (Nereson and Finnegan, 2018),

Deleted: For the hydraulic calculations described below, we use the minor axis to approximate the cross-sectional area of the boulder. Because of the proximity of boulders to the earthflow toe

For the Eel River reference site, we divided the channel into three domains where we digitized boulders separately. Along the north (river right) bank of the Eel at the toe of the Mile 201 slide is an accumulation of unsorted boulders similar to what is observed at Arroyo Hondo along the toe of Oak Ridge. However, in contrast to the Arroyo Hondo reference site, within the thalweg of the Eel River, large boulders are absent and weak sorting is apparent. Hence, we treat the population of boulders along the north bank (n = 413) as representative of the coarse fraction (> 30 cm) that is eroding out of the mélange that comprises the body of the Mile 201 earthflow, whereas we consider the thalweg to be more influenced by fluvial transport. The south (river left) bank of the Eel River at this site is similar to the north bank. However, we treat the distribution of boulders from this site (n = 706) separately because we are unsure whether this material is sourced from the Mile 201 slide or the active earthflow that enters this same location from the south (Mackey and Roering, 2011). Like in Arroyo Hondo, it is impossible to differentiate individual grains on bar surfaces away from earthflow toes in aerial imagery. Hence, again, we assume that most of the distribution of bedload that is moved by the river appears to fall below the detection limit in the imagery.

2.3 Hydrology

The USGS gage on Arroyo Hondo is located within the study reach, roughly 2 km downstream of Oak Ridge earthflow. The gage record includes 36 years of annual peak flood measurements and 248 field measurements of discharge, width and cross-sectional area during both high and low flow events. The USGS gage on the Eel River is located approximately 25 km downstream of the Highway 201 slide and roughly 12 km downsteam of the edge of the LiDAR data considered here. The gage record includes 62 years of annual peak flood measurements and 364 field measurements of discharge, width and cross-sectional area during both high and low flow events.

We calculated the recurrence period associated with the annual peak flood measurements for each gage according to standard methods (Dunne and Leopold, 1978). We then estimated the magnitude of the 2-year recurrence interval flood from the record. To accomplish this, we located the recurrence intervals that bracketed two years in the record and fit a line between these two points. Finally, using linear interpolation we determined the approximate magnitude of the 2-year recurrence interval flood, which we use as a representative high flow event in our analysis. In alluvial channels, the 2-year recurrence interval flood often corresponds to "bankfull" flow (Wolman and Miller, 1960). For this reason, the 2-year flood is commonly interpreted as the "formative" flow with respect to bankfull hydraulic geometry. Here, we use the 2-year flood, however, simply as a representative flood event that would mobilize the bed in most self-formed alluvial channels, but not necessarily in a channel overwhelmed with landslide debris.

Fortuitously, field measurements of discharge and hydraulic geometry for both gages bracket the 2-year recurrence interval flood. We divide measured cross-section area by width to quantify mean flow depth by assuming a rectangular geometry for

Deleted: data (n = 602)

Deleted:

Deleted: **Quantification of Boulder Mobility**¶
A goal of our analysis is to quantify the mobile fraction of boulders that are delivered from earthflows to channel networks. However, boulders transported by earthflows in the Franciscan Mélange are commonly comparable or greater in diameter than the depths of channels into which the earthflows empty. Consequently, below we develop an analytical model to calculate both the drag force and grain weight of partially submerged boulders in order to create an index of boulder mobility that is analogous to Shields stress but is physically valid for the case of partial submergence.¶
¶
The drag force, F_d, acting on a boulder for a given mean flow velocity, u, is given by ¶
¶
$$F_d = \frac{1}{2} C_d \rho_f u^2 a \quad \text{eq. 1}$$
¶
where C_d is a drag coefficient for boulders, estimated to be 0.36 (Bathurst, 1996), ρ_f is the density of water, and a is the cross-sectional area of the submerged portion of the boulder (Appendix 1).
¶
The partially submerged grain weight, F_g, is ¶
¶
$$F_g = v_a \rho_s g + v_s (\rho_s - \rho_f) g \quad \text{eq. 2}$$
¶
where v_a and v_s are the subaerial and submerged boulder volumes, respectively (Appendix 1), ρ_s is the density of boulders, and g is the acceleration due to gravity. The ratio of equation 1 to equation 2 is the ratio of the flow-induced drag force acting on a boulder to the partially submerged grain weight. ¶
¶
We note that the definition of Shields stress, τ^*, is also the ratio of drag force acting on a particle relative to the submerged grain weight. Assuming a spherical particle geometry, the bed shear stress, τ, acts on the cross-sectional area, $\pi(D/2)^2$, where D is, again, particle diameter. Hence, the ratio of drag force acting on a particle relative to the submerged grain weight can be written as ¶
¶
$$\frac{F_d}{F_g} = \frac{\tau \pi \left(\frac{D}{2}\right)^2}{\frac{4}{3}\pi \left(\frac{D}{2}\right)^3 g(\rho_s - \rho_f)} \quad \text{eq. 3}$$
¶
which simplifies to¶
¶
... [2]

Deleted: (https://waterdata.usgs.gov/usa/nwis/uv?11173200)

Deleted: ¶
¶

Deleted: (https://waterdata.usgs.gov/ca/nwis/uv?site_no=11475000)…

Deleted: (Dunne and Leopold, 1978).

Deleted: (Wolman and Miller, 1960).

Deleted: We divide measured discharge by measured cross-section area for each gage record in order to quantify mean flow velocity for each measurement. We alsoWe

Deleted: .

each gage. We then plotted mean flow depth versus discharge for each record. The relationships between discharge and flow depth was well fit with a power-law relationship for the Eel River record. Hence for this record, we simply use the best-fitting power law relationship to find the mean depth associated with the two-year recurrence interval flood, as well as for the maximum flood discharge during which field measurements were made. For Arroyo Hondo, a power law does not fit the relationship between discharge and flow depth at the discharges near the two-year recurrence interval flood. Consequently, for this record we used a linear fit for discharges greater than 20 m^3/s, which fits the data well in this region. We then apply this linear fit in order to determine the mean flow depth associated with the 2-year recurrence interval flood on Arroyo Hondo, as well as for the maximum flood discharge during which field measurements were made

2.4 Landslide Identification

For the Eel River site, we use the landslide mapping of Mackey and Roering (2011), who identified 122 active individual earthflows within the Eel River study site using historical aerial photos (Fig. 4). More recent studies using optical images and radar interferometry show that the majority of these landslides are still active (Bennett et al., 2016a; Bennett et al., 2016b; Handwerger et al., 2015)

For Arroyo Hondo and Alameda Creek we used a combination of airborne synthetic aperture radar interferometry (InSAR), LiDAR topography, and field reconnaissance to identify slow landslides that are either currently active, or, have been active in the recent geomorphic past.

Based on our own field reconnaissance in the area, as well as through interpretation of LiDAR-derived topographic maps, we have identified several large earthflows within the field area that clearly impinge on the channels of Arroyo Hondo and Alameda Creek (Fig. 2 and Fig. 3). We also process radar interferometry data from the airborne NASA Uninhabited Aerial Vehicle Synthetic Aperture Radar (UAVSAR) platform to identify active landslides between 2009 and 2017 (Appendix 1). UAVSAR operates with a L-Band radar wavelength (~ 24 cm) and collects data at this location approximately 2 times per year along track 23503 (aircraft moving at heading 230° and looking at 140°). We processed 31 interferograms using the InSAR Scientific Computing Environment (ISCE) software package developed at JPL/Caltech and Stanford. We remove topographic contributions to the phase using a 12 m DEM from the DLR TanDEM-X satellites. We also reduce InSAR phase noise using a standard power spectral filter with a value of 0.5 (Goldstein and Werner, 2018). Finally, we selected 7 high quality interferograms (i.e., minimal unwrapping errors, high coherence) to compute average line-of-sight (LOS) velocity map for landslides within the study area.

3 Results

3.1 Long Profile and Valley Width

Deleted: and mean flow velocity versus discharge

Deleted: velocity and discharge and

Deleted: were both

Deleted: relationships

Deleted: velocity and mean

Deleted: .

Deleted: relationships

Deleted: velocity and discharge and

Deleted:

Deleted: and mean velocity

Deleted: .

Deleted: 5

Deleted: For the Eel River site, we use the landslide mapping of Mackey and Roering (2011), who identified 122 active individual earthflows within the Eel River study site using historical aerial photos (Figure 4). More recent studies using optical images and radar interferometry show that the majority of these landslides are still active (Bennett et al., 2016a; Bennett et al., 2016b; Handwerger et al., 2015). ¶ ¶

Deleted: Figure

Deleted: ,

Deleted: 2

Deleted: 230 deg

Deleted: 140 deg

Deleted: (Rosen et al., 2012).

Deleted: (Goldstein and Werner, 1998). Finally, we selected 7 high quality interferograms (

Figures 5A, 6A, and 7A show elevation long profiles of Arroyo Hondo, Alameda Creek, and the Eel River, respectively. Also indicated on the figures are the locations where landslides intersect river channels, as shown in Figures 2-4. For the Eel River, landslide locations come from Mackey and Roering (2011). For Alameda Creek, landslide locations are, again, based on a combination of field reconnaissance, LiDAR interpretation, and InSAR.

Figures 5B-C and 6B-C show detrended long profiles and valley width (normalized to the mean for each river) respectively for Alameda Creek and Arroyo Hondo. For both channels, mapped landslide locations coincide with locations along the river marked by rapid changes in valley width from wide upstream to narrow downstream and large steps in the elevation long profile that separate anomalously low gradient reaches upstream from anomalously steep reaches downstream. We also note that the sharpest river slope increase associated with earthflows along Alameda Creek and Arroyo Hondo occurs at Oak Ridge earthflow, which is the only failure in the region that is both currently active and coupled to a river channel (Arroyo Hondo) according to InSAR (Fig. 2 and Fig. 3) and feature tracking (Nereson and Finnegan, 2019).

In contrast, Figures 7B-C show that active landslides along the Eel River have no obvious impacts on long profile morphology and valley widths. At no location along the Eel River section is the amplitude of the detrended river elevation profile larger than the 2-year flow depth, suggesting that most of the residual elevation is related to gravel bars, which are abundant along the reach in question. In addition, except for one spot along the Eel River section, valley bottom width is always less than a factor of two greater than the mean.

3.2 Boulder Size Distributions

Figure 8 shows empirical cumulative distribution functions (CDFs) of the intermediate axis of boulders mapped at the toe of Oak Ridge Earthflow, and for the right and left banks of the Eel River at the toe of the Mile 201 slide. Although the distributions diverge below ~ 1 m, the curves are quite similar for boulders larger than 1 m. A two-sample Kolmogorov-Smirnov test for the portions of each of the three measured boulder distributions above 1 m is unable to reject the hypothesis (at the 5% significance level) that the three boulder populations are drawn from the same distribution. For the Eel River, the median measured boulder size is 1.02 m and the 84th percentile is 1.90 m. For Arroyo Hondo, the median measured boulder size is 0.82 m and the 84th percentile is 1.83 m.

3.3 Hydrology

Figures 9 and 10 show calculated mean flow depths based on field measurements of channel width and cross-section area for each gage. As noted earlier, the two year recurrence interval event (shown in red in each figure) falls within the range of field measurements for the two sites, making accurate interpolation of the characteristic two year recurrence interval depth straightforward. Table 1 reports both the 2-year and largest measured mean flood depths for each gage.

Deleted: measured channel slope

Deleted: from

Deleted: slope

Deleted: to high slope

Deleted: Figure

Deleted: ,

Deleted: (Nereson and Finnegan, 2018).

Deleted: slopes

Deleted: does the channel slope increase by a factor

Deleted: two

Deleted: the study region, and

Deleted: also

Deleted: 9A

Deleted: 10A

Deleted: recurrence interval plotted against discharge for measured peak flows for the two reference gagescalculated mean

Deleted: Arroyo Hondo and the Eel River. Also shown in Figures 9B-C and 10B-C are …

Deleted: mean depth and velocity, respectively, for the two gages plotted as a function of discharge.channel width and cross-section

Deleted: depths and velocities

Deleted: these characteristic values

3.4 Quantification of Sediment Size Mobility Threshold.

We rearrange the Shields equation to solve for the threshold gravel size that can be moved assuming all of the shear stress acting on the channel bed is available to transport sediment:

$$D = \frac{\tau}{(\rho_s - \rho) g \tau^*_c} \quad (1)$$

In equation 1, D represents gravel diameter, τ is the mean channel bed shear stress, ρ and ρ_s are the density of water and sediment, respectively, g is the acceleration due to gravity and τ^*_c is the critical Shields stress. τ is calculated via the depth slope product, ρghs, where h is mean flow depth and s is channel slope. For the Arroyo Hondo USGS gage, the threshold gravel diameter associated with a two-year flood is 0.31 m. For the largest recorded flood at the gage, the threshold gravel diameter is 0.51 m (Fig. 8). For the Eel River gage, the threshold gravel diameter associated with a two-year flood is 0.22 m. For the largest recorded flood at the gage, the threshold gravel diameter is 0.32 m (Fig. 8).

We note that these estimates ignore the possible morphodynamic feedbacks that might results from the deposition of large boulders in a channel. On the one hand, landslide derived boulder deposits are steep relative to points upstream and downstream (Fig. 5A and Fig. 6A), suggesting that the deposition of landslide debris might lead to conditions more favorable to coarse sediment transport. On the other hand, large boulders exert substantial drag on the flow, which can completely offset increases in coarse sediment transport capacity due to the steeper slopes of boulder cascades (Schneider et al., 2016). For this reason, we simply consider the coarse sediment transport capacity of the river at the gage sites as an index of the river's ability to move coarse landslide-derived debris independent of changes in bed morphology caused by that debris.

4 Discussion & Conclusions

4.1 What Controls Valley Blocking?

Analysis of valley widths and river long profiles in Alameda Creek and Arroyo Hondo shows a very consistent picture in which landslides that intersect the channel force tens of meters of gravel aggradation for kilometers upstream, leading to apparently long-lived sediment storage and channel burial at these sites (Fig. 5A-C and Fig. 6A-C). In contrast to Arroyo Hondo and Alameda Creek, the Eel River does not display knickpoints at or aggradation upstream of locations where earthflows impinge on the channel, such as at the Highway 201 slide (Fig. 7A-C). Because of the similar mass wasting processes operating in the two study sites, we can identify no obvious explanation based on landslide processes alone for the paucity of evidence for valley blocking on the Eel River site. Indeed, all else being equal, we would expect more evidence for valley blocking at the Eel River site given the much greater density of active slow landslides there compared to the Arroyo Hondo and Alameda Creek sites. Given this apparently strong difference in the response of these two river systems

Deleted: Boulder

Deleted: Using equations 1-2, we calculate the mobility of the range of boulder sizes for the two reference gage sites. The results of this analysis are plotted in Figure 11A, which shows that for a two year recurrence interval flood, the boulder mobility threshold for the Eel River is ~ 4.9 m, which is approximately the 99th percentile grain size for landslide derived boulders. For Arroyo Hondo, the boulder mobility threshold is ~ 2.4 m, which is approximately the 90th percentile grain size for landslide derived boulders. These calculated mobility thresholds are also plotted on Figure 8. Given that the choice of a specific mobility threshold is somewhat arbitrary, we also plot in Figure 11B the relative mobility of boulders in the Eel River compared to Arroyo Hondo. This analysis shows that depending on grain size, boulders in the Eel are ~1.8-2.6 times more easily mobilized than in Arroyo Hondo for a two-year recurrence event. ¶

¶

Notably, although only the upper 10% of the CDF for Arroyo Hondo is immobile, this portion of the distribution nevertheless represents approximately 80% of the total volume of landslide material shed into Arroyo Hondo (Figure 12). On the Eel River, the immobile upper 1% of the CDF of boulder sizes, by contrast, represents only approximately 20% of the volume of landslide material shed into the Eel River (Figure 12). This dramatic contrast in the volume of immobile material that is shed into each of the two channels is illustrated in Figures 13 and 14, which identify in satellite imagery the individual boulders that are above the 2-year recurrence interval mobility threshold for the two reaches, calculated from equations 1-2. Whereas on the Eel River (Figure 14), immobile boulders are sparsely distributed and generally confined to the edges of the channel, on Arroyo Hondo the immobile boulders comprise clusters that span the entire channel (Figure 13)….

Deleted: Figures

Deleted: ,

Deleted: Figure 7A-C).

to similar hillslope forcing, below we explore several potential explanations based on fluvial geomorphology for the apparent resilience of the Eel River site to valley blocking by slow landslides

4.2 Coarse Sediment Transport Capacity

Deleted: Analysis of

The results of our gravel mobility calculations (Table 1) show that boulders delivered by earthflows should be immobile once delivered to river channels at both study locales. Only the very left tail of the size distribution of boulders approaches the threshold for gravel mobility in both channels during even the largest flood (> 2 year recurrence) for which field data exist at each gage (Fig. 8). That said, boulders are relatively more immobile for a given Shields stress compared to gravel (Prancevic and Lamb, 2015). Hence, it's entirely plausible that the entire distribution of boulder sizes delivered by earthflows is immobile once delivered to channels in both locations. This interpretation is supported by the fact that gravel bars downstream of the two reference earthflow sites do not contain boulders, and typically do not contain clasts that are even discernable above the ~ 30 cm resolution of the imagery. In addition, from examination of historical aerial photography in Google Earth for both locations, we were unable to see unambiguous evidence for mobile boulders even following very wet winters with large recorded flood events.

4.3 Coarse Sediment Supply

Given the relatively short time period covered by the gage data used in the mobility analysis, we acknowledge the possibility that large and infrequent floods move boulders over very long timescales (Cook et al., 2018). With this possibility in mind, here we consider landslide sediment supply relative to transport capacity as a potential driver of the differences in apparent sensitivity to landslide blocking observed between our two study sites. Because the Eel River is ~ 10 times wider than Arroyo Hondo, it has a much larger coarse sediment transport capacity than Arroyo Hondo just by virtue of its width. Hence, it's possible that the resilience of the Eel River to earthflow blocking is a consequence of its larger width and hence volumetric transport capacity. To test this, we used data from Mackey and Roering (2011) to calculate the volumetric sediment flux per unit river width of the Boulder Creek Earthflow, which is the largest earthflow on the Eel River (Fig. 4). We compare this calculation to the volumetric flux per unit river width associated with Oak Ridge Earthflow. The latter is calculated using the mean velocity of Oak Ridge earthflow (2.15 m/yr) (Nereson and Finnegan, 2019) multiplied by the width of the earthflow (~ 100 m) and the depth (~ 8 m), as reported from electrical resistivity surveys of the slide (Murphy et al., 2018). Although the Boulder Creek earthflow has an order of magnitude larger volumetric flux (~ 15,000 m^3/yr) than Oak Ridge earthflow (1700 m^3/yr), the Eel River has an order of magnitude larger channel width (125 m) than Arroyo Hondo (12 m). Hence, earthflow fluxes per unit channel width at the two sites are nearly identical, ~140 m^3/m for Arroyo Hondo and ~130 m^3/m for the Eel River. Despite this similarity, there is no evidence of blocking in the long profile of the Eel River at the location of the Boulder Creek slide (~ km 18 in Fig. 7A), whereas the channel of Arroyo Hondo is clearly blocked at Oak Ridge (Fig. 5). For this reason, we also rule out boulder supply relative to transport capacity as a likely driver of the observed morphological differences on the two rivers.

4.4 Channel Width and Seasonal Earthflow Displacement

An alternative explanation for the resilience of the Eel River to landslide blocking may be related to differences in channel width at both sites relative to typical seasonal displacements of earthflows. Figure 11 shows a histogram of seasonal earthflow displacement in the Franciscan mélange from Nereson and Finnegan (2019), who used a physically-based model to interpolate between 22 air photos of Oak Ridge earthflow, and Kelsey (1978), who used stakes to directly measure displacement on six earthflows in the Van Duzen River watershed in northern California between 1973 and 1976. Notably, the distribution of displacements, which is well fit with an exponential distribution with a mean annual displacement of ~ 4 m, contains the channel width of Arroyo Hondo (Fig. 11). By contrast, the channel width of the Eel River is ~ 5 times larger than the largest annual displacement in the distribution. Thus, during wet winters with large displacements, earthflows are capable of surging across the entire channel of Arroyo Hondo. In contrast, on the Eel River even large earthflow surges can impinge on but can't cross the active channel. In support of this interpretation, satellite imagery shows that immobile earthflow-derived boulders are generally confined to the edges of the channel on the Eel River (Fig. 12) where at each bank an active earthflow enters the Eel River. By contrast, immobile earthflow-derived boulders jam the entire channel on Arroyo Hondo (Fig. 13). We interpret this striking difference in channel morphology as an indication of the ability of earthflows to cross and hence deposit boulders within the entire width of Arroyo Hondo.

The contrasting long profile and channel morphology of the two reference locations thus suggests that the formation of valley blockages by earthflows is very sensitive to the width of river channels relative to the characteristic displacement of earthflows. In this way, channels where landslides can cross the channel may act like step-pool channels, where channel spanning, landslide-derived boulder jams locally impede coarse sediment transport. In support of this view, the observations of Golly et al. (2017) and (Brummer and Montgomery, 2006) directly linked channel spanning boulder jams to channel spanning landslides in two mountainous settings. According to flume experiments (Zimmermann et al., 2010), particle jams become much more likely when the channel width is less than six times the 84th percentile of the grain size distribution. Not coincidentally, bulk friction angle (and hence stability) of chains of clasts is larger for smaller chains, with an inflection in the relationship between frictional stability and number of clasts at around 6 grains (Booth et al., 2014). Notably, the ratio of channel width to the 84th percentile diameter of earthflow-derived boulders on Arroyo Hondo is ~ 6, suggesting that Arroyo Hondo and Alameda Creek are in a regime where they are much more susceptible to jamming once boulders are deposited on their beds. This interpretation also agrees with Costa and Schuster (1988), who found that valley width is a clear control on landslide dam formation because it is easier to block a narrow valley than a wide valley.

The fact that the Eel River does not show evidence for valley blocking likely reflects that fact that the channel is always able to flow around the toe of earthflows when they impinge on river channels. In addition, the ratio of channel width to the 84th percentile diameter of earthflow-derived boulders on the Eel River is ~ 65, which is well beyond the threshold associated

Deleted: sparsely distributed and

Deleted: Figure 14), whereas

Deleted: comprise clusters that

Deleted: Figure

Deleted: This

Deleted: implies that the Eel River is apparently capable of transporting most earthflow derived blocks, whereas Arroyo Hondo is not. This inference is supported by our mobility analysis, which shows that 80% of the volume of coarse landslide material delivered to Arroyo Hondo is immobile, compared to only 20% on the Eel River (Figure 12).…

Deleted: The contrasting long profile and channel morphology of the two reference locations suggests that the formation of valley blockages by earthflows is very sensitive to the mobility of the coarsest fraction of sediment. In this way, landslide impacted channels may act like step-pool channels, where channel spanning boulder jams locally impede coarse sediment transport. According to flume experiments (Zimmermann et al., 2010) as well as experiments of granular flow through hoppers (To et al., 2001) and silos (Zuriguel et al., 2005), particle jams become much more likely when the channel or aperture width is approximately five grain diameters or less. Not coincidentally, bulk friction angle (and hence stability) of chains of clasts is larger for smaller chains, with an inflection in the relationship between frictional stability and number of clasts at around 5 grains (Booth et al., 2014). Notably, the ratio of channel width to the threshold diameter for immobile boulders on Arroyo Hondo is ~5 as opposed to ~25 for the Eel River, suggesting that Arroyo Hondo and Alameda Creek are in a regime where they are much more susceptible to jamming. Moreover, once organized into jams, boulders are much harder to dislodge than when they are isolated on the bed (Prancevic and Lamb, 2015), suggesting that the process of valley blocking by boulders is governed by a positive feedback process. ¶

¶

Taken together, the results of our analysis suggest that valley blocking by earthflows is a process that is controlled by the clustering of a few boulders in a narrow channel, which can nevertheless impede coarse sediment transport, bedrock incision and trigger aggradation for km's upstream. Although we have no direct constraints on the process of landslide damming in other settings, particularly where catastrophic landslides are more common, it seems reasonable that the same processes that we identify here may also apply. Indeed, Costa and Schuster (1988) showed that valley width is a clear control on landslide dam formation because it is easier to block a narrow valley than a wide valley. In addition to this geometric effect, we speculate that channel spanning boulder jams, which will be more prevalent in narrower valleys, may also contribute to the tendency for landslide dams to form in narrow valleys.¶

¶

4.2

with jamming. That said, over their lifetimes, earthflows can travel hundreds of meters (Mackey and Roering, 2011; Nereson and Finnegan, 2019), distances that are in excess of what would be required to block the Eel River. Yet the Eel River shows no evidence for blocking, why? The matrix of earthflows in the Franciscan Mélange is very fine grained, making it easily transported in suspension by rivers (Kelsey, 1978; Mackey and Roering, 2011). We speculate that short-lived advances of earthflows into the Eel River during wet winters are countered by the ability of the river to remove the matrix of the earthflow during subsequent years, leading to a relatively stable position of the earthflow toe relative to the channel despite long term displacements that are sufficient to cross the channel. We emphasize, however, that this interpretation is only applicable to the relatively slow-moving earthflows that are plentiful in the Eel River basin. Catastrophic landslides, which can occur outside of the Franciscan Mélange along the Eel river, have dammed the Eel in at least one location during the Pleistocene, resulting in the formation of a huge landslide-dammed lake (Mackey et al., 2011).

4.5 Implications for River Incision and Landscape Evolution

The results of our analysis imply that the Eel River, and wide rivers like it, should be able to sustain vertical incision despite active earthflows. In other words, in settings where earthflow surges are small in comparison to channel width, landsliding may not represent a strong negative feedback on river incision. In contrast, in settings such as Arroyo Hondo and Alameda Creek, where surges can cross the entire channel, landsliding should represent a strong negative feedback on vertical river incision by triggering channel spanning boulder jams that force aggradation over large sections of river upstream of active landslides (Fig. 5A-C and Fig. 6A-C). Notably, this difference in sensitivity to landslide input is independent of the examined rivers' capacities to actually mobilize coarse debris.

Thus, our results imply that the narrow, lower drainage area, upper portions of earthflow-dominated catchments may be particularly prone to blocking. By inhibiting the upstream propagation of base-level signals, valley blocking earthflows may therefore promote the formation of so-called "relict topography" (Clark et al., 2006; Schoenbohm et al., 2004) where the upper portions of watersheds are unable to incise at the same rate as the mainstream. Indeed, Bennett et al. (2016a) noted that tributaries to the Eel River are choked with coarse sediment that significantly impedes river incision into bedrock, and hypothesized that earthflow-dominated catchments are prone to a so-called "landslide cover effect," which prevents or delays the upstream propagation of base-level signals, thereby leading to the formation of relict topography. Similarly, Korup et al. (2010) argued that sediment inputs from rockfalls and glaciers have suppressed river incision into the margin of the Tibetan Plateau, aiding in its apparent longevity. We note that Ouimet et al. (2007) and Shobe et al. (2016) also demonstrated a landslide cover effect via numerical modeling of bedrock river incision.

Our results are generally supportive of these perspectives and offer a simple mechanism for the instability that triggers the incisional shutdown of earthflow dominated channels. Moreover, because we identify a clear width (and thus drainage area) dependence on the susceptibility of channels to jamming from earthflow derived boulders, our results imply that tributary

Deleted: As noted in the introduction, the dependence of river incision on hillslope sediment input means that river incision, which provides the lower boundary condition for hillslopes, and landsliding, which delivers coarse sediment to channels, are coupled (Golly et al., 2017; Ouimet et al., 2007). The apparent strength of this coupling, however, varies widely. …

Deleted: larger

Deleted: landslide-derived blocks are mobilized by large floods

Deleted: most of the landslide-derived material is too large to be mobilizedsurges can cross the entire channel

Deleted: Figures

Deleted: ,

Deleted: ¶
¶
River incision at the toe of hillslopes, which both steepens hillslopes and debutresses them, is a trigger for earthflow motion (Bennett et al., 2016a; Bilderback et al., 2015; Golly et al., 2017; McKean, 1993; Nereson and Finnegan, 2018). Thus, aggradation upstream of valley blockages may indirectly hinder active landsliding by suppressing vertical incision. In addition, deep aggradation may directly cease landsliding by burying and hence buttressing the toes of active landslides by adding an additional longitudinal force that resists sliding. Indeed, buttressing of slow landslides by valley bottom aggradation is a potentially important but underappreciated process that can contribute to landslide stability in some settings (Johnson et al., 2016). ¶
¶
In addition to base-level forcing by rivers, both climate (Bennett et al., 2016b; Mackey et al., 2009; Nereson and Finnegan, 2018) and sediment supply (Mackey and Roering, 2011; Nereson and Finnegan, 2018) also govern the motion of slow landslides by modulating stresses via pore fluid pressures and landslide thickness, respectively (Iverson, 1986). For this reason it can be difficult to directly attribute landslide activity (or its absence) to a specific forcing. That said, a notableNotably, this

Deleted: between our two sites is that the Eel River site is characterized by dozens of active earthflows along the river canyon (Figure 4), whereas over a comparable length of river in Alameda Creek and Arroyo Hondo only two of the many mapped landslides are currently or historically active (Figures 2, 3), and only one is directly coupled to a river channel. It's possible that this difference reflects either the relatively drier climate of the San Francisco Bay area compared to Mendocino County or regional differences in rates of river incision and hence base-level forcing. However, it's also possible that the relative inactivity of slow landslides in Alameda Creek and Arroyo Hondo reflects the fact that valley blocking by [3]

Formatted: English (US)

Deleted: Finally

Deleted: because they lack the flow depths sufficient to transport landslide debris..

Deleted: (Clark et al., 2006; Schoenbohm et al., 2006)

Deleted:

Deleted: Moreover, because we identify a clear discharge (and thus drainage area) dependence on the susceptibility of channels to jamming from earthflow derived boulders, our results imply that … [4]

junctions are likely to mark boundaries between relict topography and actively incising canyons. In other words, landslide or debris flow derived boulder jams in narrow channels provide an alternative explanation for the phenomenon of fluvial hanging valleys, where tributary channels in steep canyons are apparently unable to incise at the rate of trunk channel incision (Crosby et al., 2007; Wobus et al., 2006).

We note that morphodynamic models for river response to landslide inputs (Croissant et al., 2017; Ouimet et al., 2007; Shobe et al., 2016)generally assume that landslide debris is ultimately transportable by rivers. This is an assumption, however, that our results do not necessarily support. One obvious question raised by our observations therefore is how channels that are blocked with earthflow debris nevertheless manage to incise bedrock canyons over geologic timescales? While this question is not answerable with the results of this study, our observations point to two field-testable hypotheses. Central to both hypotheses is the fact that earthflows are fundamentally transient in nature and their activity must punctuate long periods of dormancy (Mackey and Roering, 2011).

1) We have observed epigenetic gorges (Ouimet et al., 2008) at several locations (AL3, unnamed slide between AL3 and AL2) where active earthflows impinge on Alameda Creek. This observation suggests that narrow channels in the Franciscan Mélange that are buried in debris may eventually incise around the margins of boulder jams, perhaps during periods of earthflow dormancy when boulders are no longer being input into channels. Epigenetic gorge formation might be a particularly important process in the Franciscan Mélange, where the clasts in the mélange, which accumulate in channels, are typically much harder than the matrix. Hence, bedrock river incision in the mélange may occur far more efficiently than boulder transport.

2) Alternatively, it's possible that large boulders are mobilized during extremely large but very infrequent flood events (e.g., Cook et al., 2018). In this case, during periods of earthflow dormancy, infrequent boulder transport events could result in the slow erosional removal of the valley blockage. In support of this view, we note that the knickpoint located at Oak Ridge Earthflow, which is currently active, is much steeper than knickpoints located at dormant earthflows in the region (Fig. 5 and Fig. 6). This suggests that over time the valley blockages may diffuse due to sediment transport. The process of boulder transport in this scenario would likely be aided by abrasion (and hence size reduction) of boulders in place from suspended sediment.

Deleted: We note that Shobe et al. (2016) suggested that detachment-limited channels where boulders are fed from hillslopes will naturally evolve to have greater stresses in order to compensate the extra drag from boulders. Finnegan et al. (2017) also showed a clear relationship between bedrock channel slope and grain diameter and suggested it was due to the transport-limited nature of erosion in the setting they examined. Finally, Ouimet et al. (2007) argued that channels that are prone to landsliding should evolve to be steeper because of the decreased erosional efficiency associated with landslide burial (essentially the "landslide cover effect" of Bennett et al., 2016a). ¶

¶

Given these results, it is tempting to interpret the difference in boulder transport capacity on the Eel River relative to Arroyo Hondo and Alameda Creek from the perspective of these studies, which would imply that the Eel River has evolved to compensate earthflow boulder fluxes, whereas Arroyo Hondo and Alameda Creek have not. However, we note that bankfull stresses are actually very similar on Arroyo Hondo compared to the Eel River (Table 1). This serves to illustrate the fact that it is the Eel River's deep flows, not its slope, that enables it to move very large boulders, as is clear from equation 1, where the cross-sectional area of the boulder exposed to the flow (which is a function of flow depth) governs the boulder drag force. Because the flow depth is largely determined by drainage area (Leopold and Maddock Jr, 1953), it cannot respond in a simple way to sediment supply. Hence, our results suggest that the bedrock channels studied here have not evolved in an obviously identifiable way to boulder inputs. Rather, our results imply that the capacity (or lack thereof) to move earthflow-derived boulders is largely an accident of drainage area. Notably, we have observed epigenetic gorges (Ouimet et al., 2008)) at several locations where active earthflows impinge on Alameda Creek, which suggests that channels in the Franciscan Mélange may simply incise around the margins of episodically-delivered (e.g., Mackey and Roering, 2011) earthflow boulder deposits. Given the extremely weak matrix of the Franciscan Mélange, we speculate that the extra bedrock incision that is necessitated by period epigenetic gorge formation may have little impact on the time-integrated erosional efficiency of these channels. That said, without much more detailed field studies, we can only conjecture.We note that morphodynamic models for river

Formatted: Font: Bold

Acknowledgements

This work was supported by a National Science Foundation (NSF) Graduate Research Fellowship awarded to A.L.N. and the Geomorphology and Land Use Dynamics Program of NSF (EAR-1658800 and EAR-1613122 to N.J.F.). We thank Zhen Liu and the UAVSAR flight and data processing teams for their help with acquiring and processing the data. Part of this research was sponsored by the NASA Earth Surface and Interior focus area and performed at the Jet Propulsion Laboratory, California Institute of Technology. A.L.H's research was supported by an appointment to the NASA Postdoctoral Program at the Jet Propulsion Laboratory, administered by Universities Space Research Association under contract with NASA. We thank the San Francisco Public Utilities Commission and Russ Fields for site access. In addition, we thank Roman DiBiase and Jeff Prancevic, as well as an anonymous reviewer, for comments that improved and fundamentally reshaped aspects of this manuscript.

Appendix 1, UAVSAR Acquisitions and InSAR Pairs

UAVSAR Acquisition	20090220	20091120	20100511	20100115	20100116	20111114	20121102	20130507
20090220								
20091120								
20100511								
20100115								
20100116								
20111114								
20121102								
20130507								

Formatted: Font: Times New Roman, 10 pt, Font color: Auto, Pattern: Clear

Deleted: ¶

Deleted: **- Submerged Cross-Sectional Area and Volume of Boulders**¶

Figure A1 provides a sketch of the geometry employed in the model. In Figure A1, h is flow depth, u is mean flow velocity into the page, a is the submerged cross-sectional area of the boulder (shown by shaded region), r is boulder radius.¶

b, is given by:¶

$$b = \frac{D}{2} - (D - h) \quad \text{eq. 1a}$$

for the case where h >= D/2, where h is flow depth and D is boulder diameter. Alternatively, for the case where h < D/2, b is given by¶

$$b = h \quad \text{eq. 1b}$$

c is then calculated via the pythagorean theorem:¶

$$c = 2\left(\left(\frac{D}{2}\right)^2 - b^2\right)^{\frac{1}{2}} \quad \text{eq. 2a}$$

for the case where h >= D/2. Alternatively, for the case where h < D/2, c is given by¶

$$c = 2\left(\left(\frac{D}{2}\right)^2 - \left(\left(\frac{D}{2}\right) - b\right)^2\right)^{\frac{1}{2}} \quad \text{eq. 2b}$$

θ, measured in radians, is given by,

$$\theta = \sin^{-1}\left(\frac{c}{D}\right) \quad \text{eq. 3}$$

Finally, the area of the submerged portion of the boulder, a, is given by

$$a = \pi\left(\frac{D}{2}\right)^2 - \left(\frac{1}{2}\left(\frac{D}{2}\right)^2(\theta - \sin\theta)\right) \quad \text{eq. 4a}$$

for the case where h >= D/2. Alternatively, for the case where h < D/2, a is given by¶

... [5]

Formatted: Font: Not Bold

		2-Year Mean Flow Depth (m)	Largest Field Measured Flow, Depth (m)	Channel Slope	2-Year Mean Bed Shear Stress (Pa)	Largest Field Measured Flow, Mean Bed Shear Stress (Pa)	2-Year Gravel Mobility Threshold (m)	Largest Field Measured Flow, Mobility Threshold (m)	Channel Width (m)
Eel River		7.1	10	0.0026	180	255	0.22	0.32	125
Arroyo Hondo		1.6	2.8	0.016	250	431	0.31	0.53	12

Table 1: Channel characteristics for the two reference locations.

Deleted: ¶ ... [6]
Formatted ... [14]
Formatted ... [18]
Formatted Table ... [7]
Deleted: Two Year Discharge¶ ... [8]
Deleted: Two
Deleted: Drainage Area (km^2)
Formatted ... [9]
Deleted: Two Year Mean Velocity (m/s)
Deleted: Two
Inserted Cells ... [23]
Inserted Cells ... [24]
Inserted Cells ... [25]
Formatted ... [15]
Formatted ... [16]
Formatted ... [17]
Formatted ... [12]
Formatted ... [13]
Formatted ... [10]
Formatted ... [21]
Formatted ... [11]
Formatted ... [22]
Formatted ... [19]
Formatted ... [20]
Formatted ... [26]
Deleted: 2826
Formatted ... [27]
Deleted: 3.0
Formatted ... [28]
Deleted: 5547
Formatted ... [29]
Formatted ... [30]
Deleted: 92
Formatted ... [31]
Deleted: 4
Formatted ... [32]
Deleted: 200
Formatted ... [33]

Figure 1: Overview of the study region. Franciscan Complex rocks are shown in purple. Red boxes indicate the locations of the two field locales.

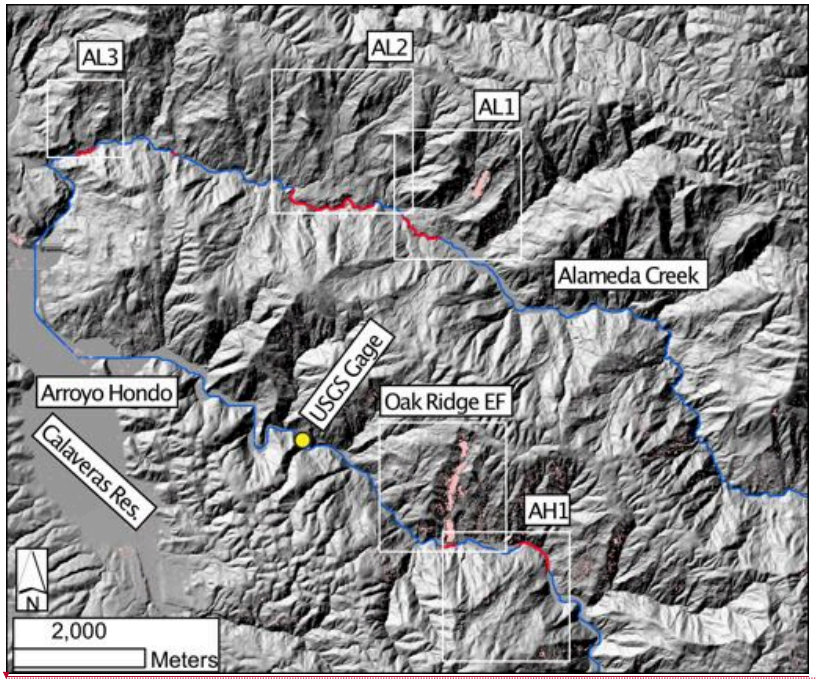

Deleted: ¶

Formatted: Justified

Figure 2: Shaded relief map of the study reaches of the Alameda Creek and Arroyo Hondo watersheds. White boxes highlight large mapped earthflows in the study area, which are shown in more detail in Figure 3. Rivers channels are indicated with blue lines, except where they intersect active earthflows (red lines). Areas of light red shading show regions where the InSAR analysis indicated line-of-site velocities in excess of 3 cm/yr.

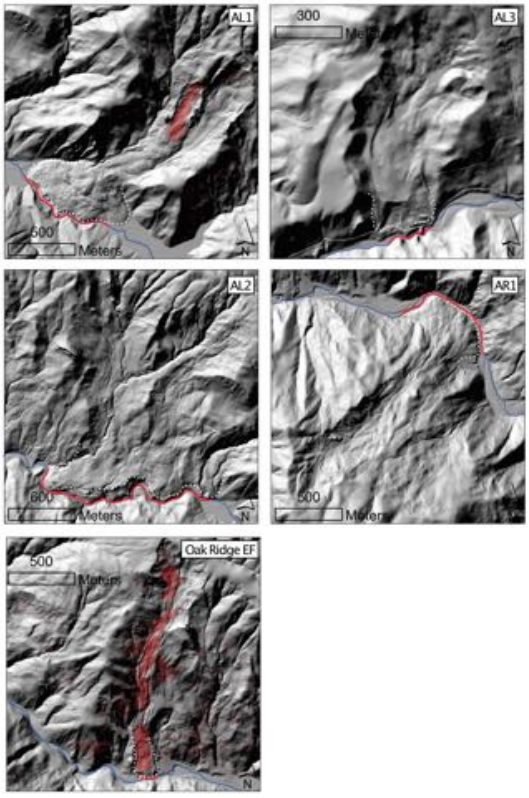

Deleted: ¶
¶
¶
¶
<object>¶
¶
¶
¶
¶
¶
¶
¶
¶
¶
¶
¶
¶
¶
¶
¶
¶
¶
¶
¶
¶
¶
¶
¶
¶
¶
¶
¶
¶
¶
¶
¶

Formatted: Font: Bold

Figure 3: Shaded relief maps of three large earthflows on Alameda Creek (A-C) and two on Arroyo Hondo (D-E). White dashed lines indicated the mapped edge of earthflow toes, and red lines indicate where river channels (shown

in blue) intersect earthflows. Areas of red shading show regions where the InSAR analysis indicated line-of-site velocities in excess of 3 cm/yr.

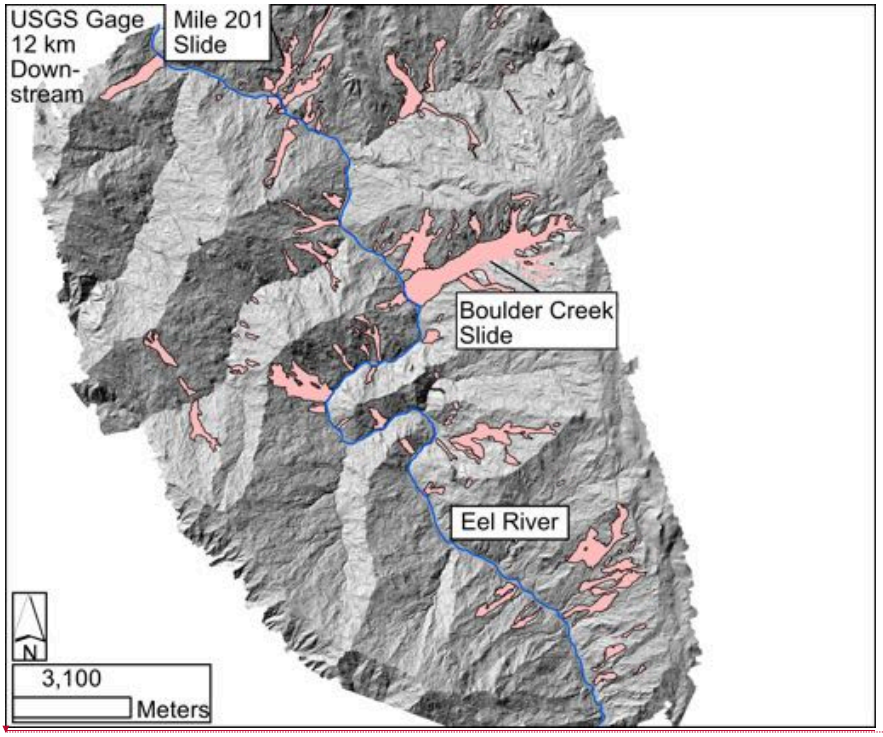

Deleted: ¶
<object>¶

Figure 4: Shaded relief map of the Eel River site. The thalweg of the Eel River is shown in blue. Areas of red shading are active earthflows mapped by Mackey and Roering (2011). River flow is from the lower right to upper left.

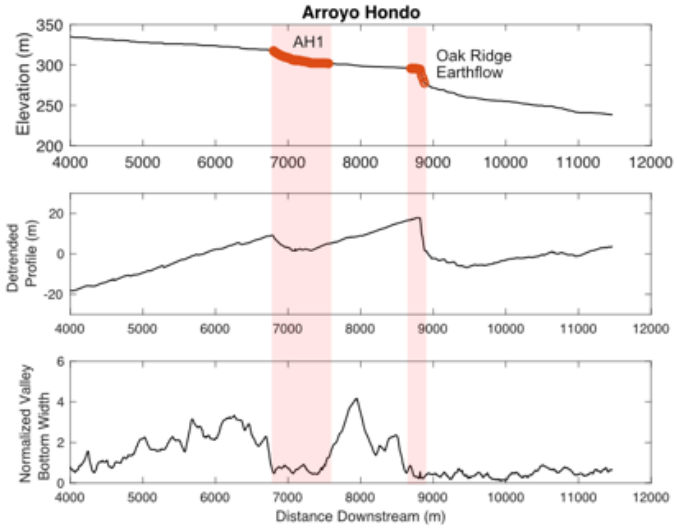

Figure 5: A) Elevation long profile of Arroyo Hondo. Locations where the channel intersects mapped earthflows in Figures 2 and 3 are shown in red and labeled. B) Detrended elevation profile of Arroyo Hondo for the reach shown in Figure 5A. C) Valley bottom width Arroyo Hondo normalized by the mean valley bottom width over the reach shown in Figure 5A. In A-C, the red boxes highlight earthflow impacted reaches.

Deleted: ¶
¶
¶
<object>¶
¶
¶
¶
¶
¶
¶
¶
¶
¶
¶
¶
¶
¶
¶

Deleted: Channel slope on
Deleted: normalized by the mean slope over
Deleted: vertical dotted
Deleted: lines
Deleted: the upstream edge of mapped earthflows

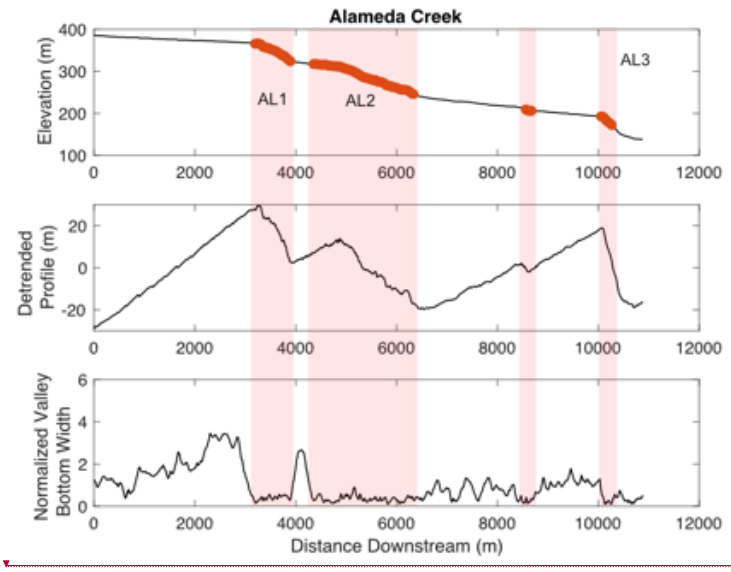

Deleted: ¶
¶
¶
¶
¶
¶
¶
<object>¶
¶
¶
¶
¶
¶
¶
¶
¶
¶
¶
¶
¶
¶
¶

Figure 6: A) Elevation long profile of Alameda Creek. Locations where the channel intersects mapped earthflows in Figures 2 and 3 are shown in red and labeled. B) Detrended elevation profile of Alameda Creek for the reach shown in Figure 6A. C) Valley bottom width Alameda Creek normalized by the mean valley bottom width over the reach shown in Figure 6A. In A-C, the vertical dotted red lines highlight the upstream edge of mapped earthflows. In A-C, the red boxes highlight earthflow impacted reaches.

Deleted: Channel slope on

Deleted: normalized by the mean slope over

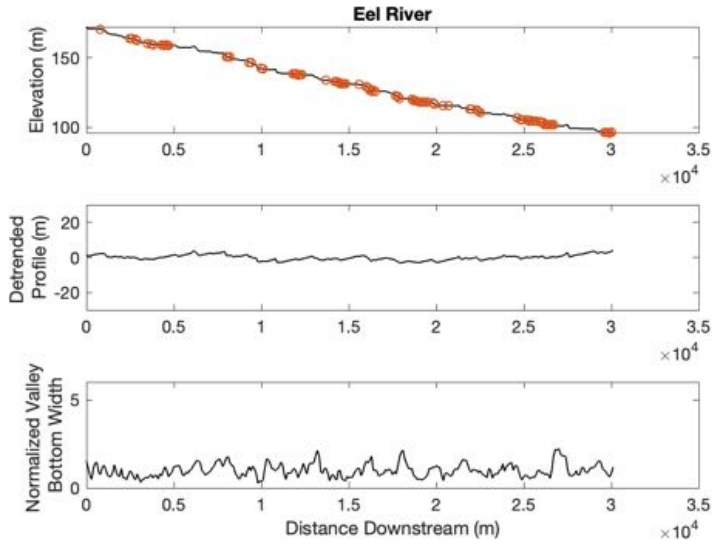

Deleted: ¶

<object>¶

Figure 7: A) Elevation long profile of the Eel River. Locations where the channel intersects mapped earthflows in Figure 4 are shown in red. B) Detrended elevation profile of the Eel River for the reach shown in Figure 7A. C) Valley bottom width on the Eel River normalized by the mean valley bottom width over the reach shown in Figure 7A. Red rectangles highlight earthflow impacted reaches in A-C.

Deleted: Channel slope on

Deleted: normalized by the mean slope over

Formatted: Centered

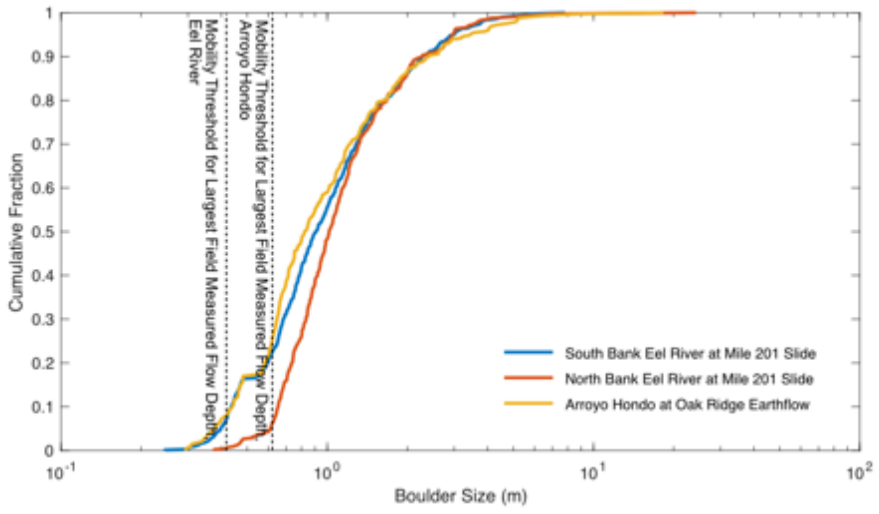

Figure 8: Empirical cumulative distribution functions for the intermediate axes of earthflow-derived boulders at the toe of Oakridge Earthflow and for the banks of the Eel River site at the Mile 201 Slide. The vertical lines indicate the threshold mobile grain diameter for the largest field measured flow depths at each site (see Figure 9 & 10).

Deleted: ¶
¶
¶
¶
¶
¶
<object>¶
¶
¶
¶
¶
¶
¶

Formatted: Font: Bold

Deleted: two year recurrence interval floods at the two reference sites.the largest field measured flow depths at each site

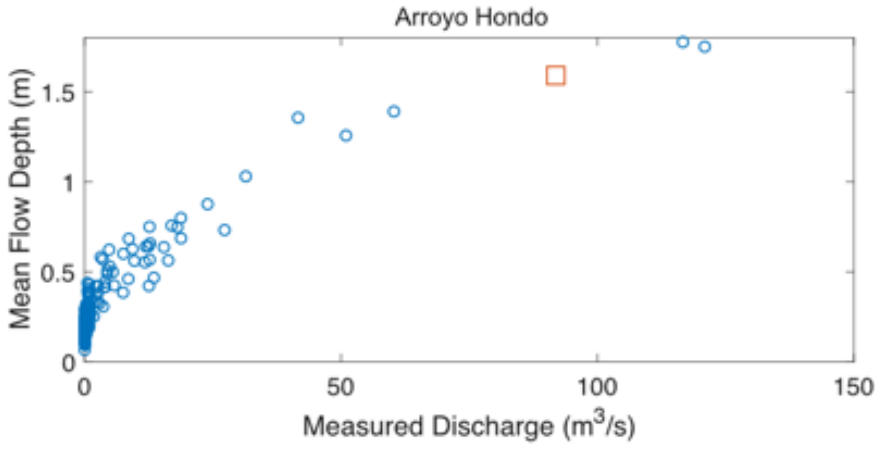

Figure 9: Mean flow depth versus measured discharge for the USGS Arroyo Hondo gage. Red square indicates the interpolated two-year recurrence interval depth.

Formatted: Font: Bold

Deleted: ¶
¶
¶
¶
<object>¶
¶
¶
¶
¶
¶
¶
¶
¶
¶
¶
¶
¶
¶
¶
¶
¶
¶

Formatted: Font: Bold

Deleted: A) Recurrence interval, B) measured

Deleted: , and C) measured mean velocity

Deleted: vertical lines indicate

Deleted:

Deleted: flood magnitude

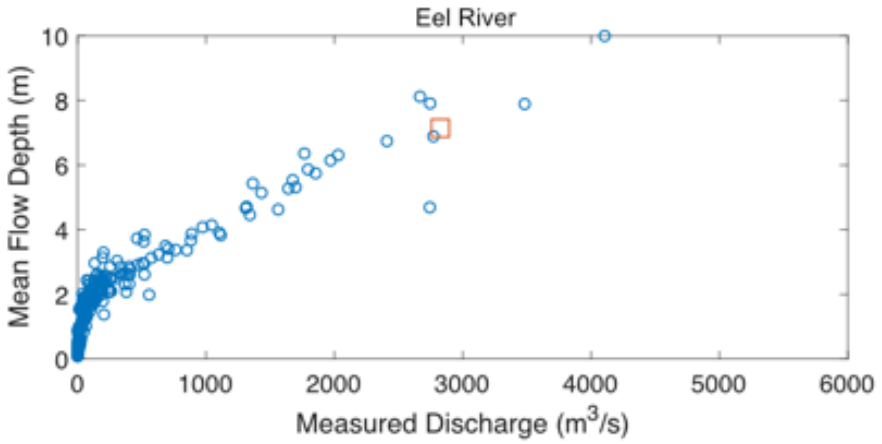

Figure 10: Mean flow depth versus measured discharge for the USGS Eel River gage at Fort Seward. Red square indicates the interpolated two-year recurrence interval depth.

Deleted: ¶

<object>¶

Deleted: A) Recurrence interval, B) measured

Deleted: , and C) measured mean velocity

Deleted: vertical lines indicate

Deleted:

Deleted: flood magnitude

Formatted: Font: Bold

Formatted: Font: Bold

Deleted: <object>¶

... [34]

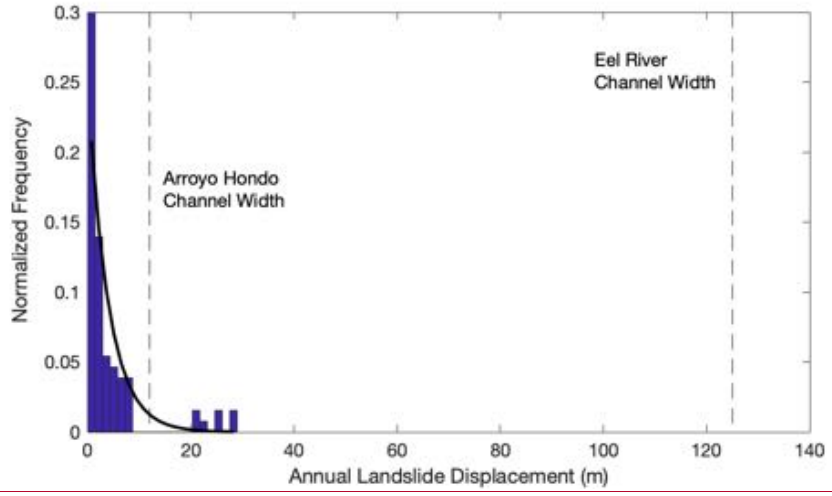

Figure 11: Normalized histogram of annual earthflow displacements in the Franciscan Mélange, data from Kelsey (1978) and Nereson and Finnegan (2019). Black line shows exponential fit between normalized frequency and displacement. Vertical dashed lines indicate the channel width of Arroyo Hondo and the Eel River.

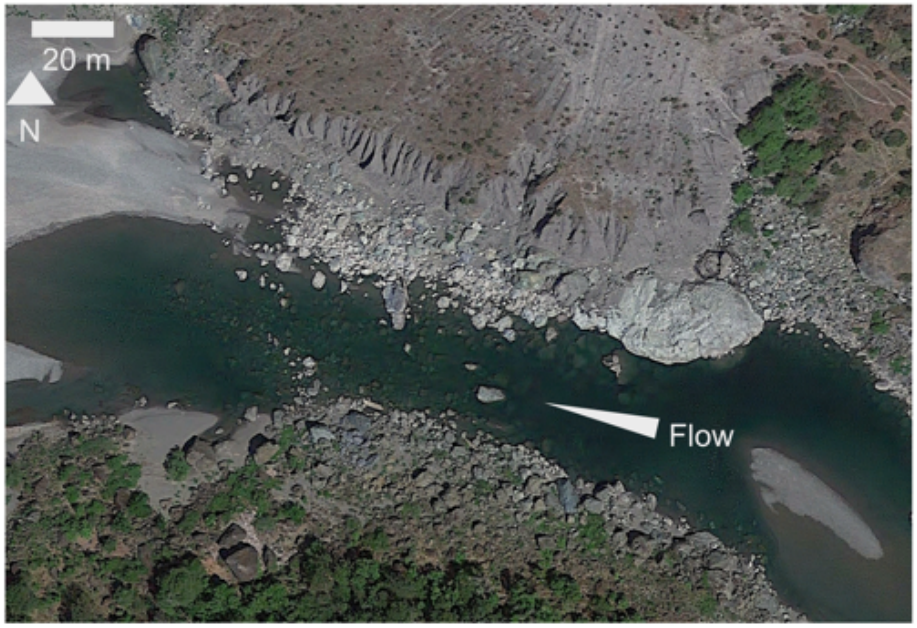

Figure 12: Google Earth satellite image of Arroyo Hondo at the toe of the Oakridge earthflow during high flow conditions, March 11, 2017. Flow is from right to left, and north is up.

Deleted: Cumulative volume fraction as a function of boulder diameter for the Mile 201 and Oakridge Earthflow sites. The dashed lines indicate the cumulative volume of material that is mobile in a 2-year recurrence interval flood for the Eel River and Arroyo Hondo.¶

¶

¶

¶

¶

¶

¶

¶

¶

¶

<object>¶

¶

¶

¶

¶

¶

¶

¶

¶

¶

¶

¶

¶

¶

¶

¶

¶

¶

¶

¶

¶

¶

Figure 13: Satellite

Deleted: . Red boxes outline boulders that, according to our analysis, are immobile in a 2-year recurrence interval event. Blue boxes outline boulders that, according to our analysis, are mobile in a 2-year recurrence interval event…

Deleted: ¶
¶
¶
¶
¶
¶
¶
<object>¶
¶
¶
¶
¶
¶
¶
¶
¶
¶
¶
¶
¶
¶

Figure 13: Google Earth satellite image of the Eel River at the toe of the Mile 201 earthflow, May 28, 2014. Flow is from right to left, and north is up. Earthflows enter the channel here on each bank, which likely explains the different colored boulders being deposited on each bank.

Deleted: 14: Satellite

Deleted: . Red boxes outline boulders that, according to our analysis, are immobile in a 2-year recurrence interval event. Blue boxes outline boulders that, according to our analysis, are mobile in a 2-year recurrence interval event…

Formatted: Font: Not Bold

References

Baum, R. L., Savage, W. Z. and Wasowski, J.: Mechanics of Earthflows, in Proceedings of the International Conference FLOWS, Sorrento, Italy., 2003.

Bennett, G. L., Roering, J. J., Mackey, B. H., Handwerger, A. L., Schmidt, D. A. and Guillod, B. P.: Historic drought puts the brakes on earthflows in Northern California: Drought Puts Breaks on Earthflows, Geophys. Res. Lett., 43(11), 5725–5731, doi:10.1002/2016GL068378, 2016.

Booth, A. M., Hurley, R., Lamb, M. P. and Andrade, J. E.: Force chains as the link between particle and bulk friction angles in granular material, Geophys. Res. Lett., 41(24), 8862–8869, doi:10.1002/2014GL061981, 2014.

Brummer, C. J. and Montgomery, D. R.: Influence of coarse lag formation on the mechanics of sediment pulse dispersion in a mountain stream, Squire Creek, North Cascades, Washington, United States, Water Resour. Res., 42(7), doi:10.1029/2005WR004776, 2006.

Bull, W. B.: Stream-terrace genesis: implications for soil development, Geomorphology, 3(3), 351–367, doi:10.1016/0169-555X(90)90011-E, 1990.

Burbank, D. W., Leland, J., Fielding, E., Anderson, R. S., Brozovic, N., Reid, M. R. and Duncan, C.: Bedrock incision, rock uplift and threshold hillslopes in the northwestern Himalayas, Nature, 379(6565), 505, doi:10.1038/379505a0, 1996.

Clark, M. K., Royden, L. H., Whipple, K. X., Burchfiel, B. C., Zhang, X. and Tang, W.: Use of a regional, relict landscape to measure vertical deformation of the eastern Tibetan Plateau, J. Geophys. Res. Earth Surf., 111(F3), doi:10.1029/2005JF000294, 2006.

Cook, K. L., Turowski, J. M. and Hovius, N.: A demonstration of the importance of bedload transport for fluvial bedrock erosion and knickpoint propagation, Earth Surf. Process. Landf., 38, 683–695, doi:10.1002/esp.3313, 2013.

Cook, K. L., Andermann, C., Gimbert, F., Adhikari, B. R. and Hovius, N.: Glacial lake outburst floods as drivers of fluvial erosion in the Himalaya, Science, 362(6410), 53–57, doi:10.1126/science.aat4981, 2018.

Costa, J. E. and Schuster, R. L.: The formation and failure of natural dams, GSA Bull., 100(7), 1054–1068, doi:10.1130/0016-7606(1988)100<1054:TFAFON>2.3.CO;2, 1988.

Croissant, T., Lague, D., Steer, P. and Davy, P.: Rapid post-seismic landslide evacuation boosted by dynamic river width, Nat. Geosci., 10(9), 680–684, doi:10.1038/ngeo3005, 2017.

Crosby, B. T., Whipple, K. X., Gasparini, N. M. and Wobus, C. W.: Formation of fluvial hanging valleys: Theory and simulation, J. Geophys. Res. Earth Surf., 112(F3), doi:10.1029/2006JF000566, 2007.

Dunne, T. and Leopold, L. B.: Water in Environmental Planning, Macmillan., 1978.

Fleming, R. W. and Johnson, A. M.: Structures associated with strike-slip faults that bound landslide elements, Eng. Geol., 27(1), 39–114, doi:10.1016/0013-7952(89)90031-8, 1989.

Gilbert, G. K.: Geology of the Henry Mountains, USGS Unnumbered Series, Government Printing Office, Washington, D.C. [online] Available from: http://pubs.er.usgs.gov/publication/70038096 (Accessed 17 April 2019), 1877.

Deleted: ¶

Bathurst, J. C., 1996, Field measurement of boulder flow drag: Journal of Hydraulic Engineering, v. 122, no. 3, p. 167-169.¶
Baum, R., Savage, W., and Wasowski, J., Mechanics of earth flows, *in* Proceedings Proceedings of the International Conference FLOWS, Sorrento, Italy2003.¶
Bennett, G. L., Miller, S. R., Roering, J. J., and Schmidt, D. A., 2016a, Landslides, threshold slopes, and the survival of relict terrain in the wake of the Mendocino Triple Junction: Geology, v. 44, no. 5, p. 363-366.¶
Bennett, G. L., Roering, J. J., Mackey, B. H., Handwerger, A. L., Schmidt, D. A., and Guillod, B. P., 2016b, Historic drought puts the brakes on earthflows in Northern California: Geophysical Research Letters, v. 43, no. 11, p. 5725-5731.¶
Bilderback, E. L., Pettinga, J. R., Litchfield, N. J., Quigley, M., Marden, M., Roering, J. J., and Palmer, A. S., 2015, Hillslope response to climate-modulated river incision in the Waipaoa catchment, East Coast North Island, New Zealand: Bulletin, v. 127, no. 1-2, p. 131-148.¶
Booth, A. M., Hurley, R., Lamb, M. P., and Andrade, J. E., 2014, Force chains as the link between particle and bulk friction angles in granular material: Geophysical Research Letters, v. 41, no. 24, p. 8862-8869.¶
Burbank, D. W., Leland, J., Fielding, E., Anderson, R. S., Brozovic, N., Reid, M. R., and Duncan, C., 1996, Bedrock incision, rock uplift and threshold hillslopes in the northwestern Himalayas: Nature, v. 379, no. 6565, p. 505-510.¶
Clark, M. K., Royden, L. H., Whipple, K., Burchfiel, B., Zhang, X., and Tang, W., 2006, Use of a regional, relict landscape to measure vertical deformation of the eastern Tibetan Plateau: Journal of Geophysical Research: Earth Surface, v. 111, no. F3.¶
Cook, K. L., Turowski, J. M., and Hovius, N., 2013, A demonstration of the importance of bedload transport for fluvial bedrock erosion and knickpoint propagation: Earth Surface Processes and Landforms, v. 38, no. 7, p. 683-695.¶
Costa, J. E., and Schuster, R. L., 1988, The formation and failure of natural dams: Geological society of America bulletin, v. 100, no. 7, p. 1054-1068.¶
Crosby, B. T., Whipple, K. X., Gasparini, N. M., and Wobus, C. W., 2007, Formation of fluvial hanging valleys: Theory and simulation: J. Geophys. Res., v. 112, no. F3, p. F03S10.¶
Dunne, T., and Leopold, L. B., 1978, Water In Environmental Planning, San Francisco, CA, W.H. Freeman and Co.¶
Finlayson, D. P., Montgomery, D. R., and Hallet, B., 2002, Spatial coincidence of rapid inferred erosion with young metamorphic massifs in the Himalayas: Geology, v. 30, no. 3, p. 219-222.¶
Finnegan, N. J., Klier, R. A., Johnstone, S., Pfeiffer, A. M., and Johnson, K., 2017, Field evidence for the control of grain size and sediment supply on steady-state bedrock river channel slopes in a tectonically active setting: Earth Surface Processes and Landforms, v. 42, no. 14, p. 2338-2349.¶
Fleming, R. W., and Johnson, A. M., 1989, Structures associated with strike-slip faults that bound landslide elements: Engineering Geology, v. 27, no. 1-4, p. 39-114.¶
Gilbert, G. K., 1877, Report on the geology of the Henry Mountains, Washington, D.C., Government Print Office, 170 p.:¶
Goldstein, R. M., and Werner, C. L., 1998, Radar interferogram filtering for geophysical applications: Geophysical research letters, v. 25, no. 21, p. 4035-4038.¶
Golly, A., Turowski, J. M., Badoux, A., and Hovius, N., 2017, Controls and feedbacks in the coupling of mountain channels and hillslopes: Geology, v. 45, no. 4, p. 307-310.¶

... [35]

Goldstein, R. M. and Werner, C. L.: Radar interferogram filtering for geophysical applications, Geophys. Res. Lett., 4035–4038, doi:10.1029/1998GL900033@10.1002/(ISSN)1944-8007.GRL40, 2018.

Golly, A., Turowski, J. M., Badoux, A. and Hovius, N.: Controls and feedbacks in the coupling of mountain channels and hillslopes, Geology, 45(4), 307–310, doi:10.1130/G38831.1, 2017.

Handwerger, A. L., Roering, J. J., Schmidt, D. A. and Rempel, A. W.: Kinematics of earthflows in the Northern California Coast Ranges using satellite interferometry, Geomorphology, 246, 321–333, doi:10.1016/j.geomorph.2015.06.003, 2015.

Handwerger, A. L., Fielding, E. J. and Huang, M. H.: Widespread increase and acceleration of slow-moving landslides in response to extreme rainfall, AGU Fall Meet. Abstr., 24 [online] Available from: http://adsabs.harvard.edu/abs/2018AGUFMEP24B..06H (Accessed 24 April 2019), 2018.

Handwerger, A. L., Huang, M.-H., Fielding, E. J., Booth, A. M. and Bürgmann, R.: A shift from drought to extreme rainfall drives a stable landslide to catastrophic failure, Sci. Rep., 9(1), 1569, doi:10.1038/s41598-018-38300-0, 2019.

Hungr, O., Leroueil, S. and Picarelli, L.: The Varnes classification of landslide types, an update, Landslides, 11(2), 167–194, doi:10.1007/s10346-013-0436-y, 2014.

Iverson, R. M. and Major, J. J.: Rainfall, ground-water flow, and seasonal movement at Minor Creek landslide, northwestern California: Physical interpretation of empirical relations, GSA Bull., 99(4), 579–594, doi:10.1130/0016-7606(1987)99<579:RGFASM>2.0.CO;2, 1987.

Keefer, D. K. and Johnson, A. M.: Earth flows; morphology, mobilization, and movement, USGS Numbered Series, U.S. G.P.O.,. [online] Available from: http://pubs.er.usgs.gov/publication/pp1264 (Accessed 21 April 2019), 1983.

Kelsey, H. M.: Earthflows in Franciscan melange, Van Duzen River basin, California, Geology, 6(6), 361–364, doi:10.1130/0091-7613(1978)6<361:EIFMVD>2.0.CO;2, 1978.

Korup, O.: Recent research on landslide dams - a literature review with special attention to New Zealand, Prog. Phys. Geogr. Earth Environ., 26(2), 206–235, doi:10.1191/0309133302pp333ra, 2002.

Korup, O., Strom, A. L. and Weidinger, J. T.: Fluvial response to large rock-slope failures: Examples from the Himalayas, the Tien Shan, and the Southern Alps in New Zealand, Geomorphology, 78(1), 3–21, doi:10.1016/j.geomorph.2006.01.020, 2006.

Korup, O., Montgomery, D. R. and Hewitt, K.: Glacier and landslide feedbacks to topographic relief in the Himalayan syntaxes, Proc. Natl. Acad. Sci., 107(12), 5317–5322, doi:10.1073/pnas.0907531107, 2010.

Larsen, I. J. and Montgomery, D. R.: Landslide erosion coupled to tectonics and river incision, Nat. Geosci., 5(7), 468–473, doi:10.1038/ngeo1479, 2012.

Mackey, B. H. and Roering, J. J.: Sediment yield, spatial characteristics, and the long-term evolution of active earthflows determined from airborne LiDAR and historical aerial photographs, Eel River, California, GSA Bull., 123(7–8), 1560–1576, doi:10.1130/B30306.1, 2011.

Mackey, B. H., Roering, J. J. and Lamb, M. P.: Landslide-dammed paleolake perturbs marine sedimentation and drives genetic change in anadromous fish, Proc. Natl. Acad. Sci., 108(47), 18905–18909, doi:10.1073/pnas.1110445108, 2011.

McLaughlin, R. J., Ellen, S. D., Blake Jr., M. C., Jayko, A. S., Irwin, W. P., Aalto, K. R., Carver, G. A., Clarke Jr., S. H., Barnes, J. B., Cecil, J. D. and Cyr, K. A.: Geology of the Cape Mendocino, Eureka, Garberville, and Southwestern Part of the Hayfork 30 x 60 Minute Quadrangles and Adjacent Offshore Area, Northern California, USGS Numbered Series, U.S. Geological Survey. [online] Available from: http://pubs.er.usgs.gov/publication/mf2336 (Accessed 1 May 2019), 2000.

Mey, J., Scherler, D., Zeilinger, G. and Strecker, M. R.: Estimating the fill thickness and bedrock topography in intermontane valleys using artificial neural networks: ESTIMATING VALLEY-FILL THICKNESSES, J. Geophys. Res. Earth Surf., 120(7), 1301–1320, doi:10.1002/2014JF003270, 2015.

Miller, S. R., Roering, J. J. and Schmidt, D. A.: Landslides, threshold slopes, and the survival of relict terrain in the wake of the Mendocino Triple Junction, Geology, 44(5), 363–366, doi:10.1130/G37530.1, 2016.

Murphy, C., Finnegan, N. J., Oberle, F. J. and Perkins, J. P.: Evidence for a Positive Feedback Between Shallow Groundwater Flow and Shear Failure in an Active Earthflow, AGU Fall Meet. Abstr. [online] Available from: http://adsabs.harvard.edu/abs/2018AGUFMEP24B..05M (Accessed 25 April 2019), 2018.

Nereson, A. L. and Finnegan, N. J.: Drivers of earthflow motion revealed by an 80 yr record of displacement from Oak Ridge earthflow, Diablo Range, California, USA, GSA Bull., 131(3–4), 389–402, doi:10.1130/B32020.1, 2019.

Ouimet, W. B., Whipple, K. X., Royden, L. H., Sun, Z. and Chen, Z.: The influence of large landslides on river incision in a transient landscape: Eastern margin of the Tibetan Plateau (Sichuan, China), GSA Bull., 119(11–12), 1462–1476, doi:10.1130/B26136.1, 2007.

Ouimet, W. B., Whipple, K. X., Crosby, B. T., Johnson, J. P. and Schildgen, T. F.: Epigenetic gorges in fluvial landscapes, Earth Surf. Process. Landf., 33(13), 1993–2009, doi:10.1002/esp.1650, 2008.

Prancevic, J. P. and Lamb, M. P.: Particle friction angles in steep mountain channels: Friction angles in mountain channels, J. Geophys. Res. Earth Surf., 120(2), 242–259, doi:10.1002/2014JF003286, 2015.

Reneau, S. L. and Dietrich, W. E.: Erosion rates in the southern oregon coast range: Evidence for an equilibrium between hillslope erosion and sediment yield, Earth Surf. Process. Landf., 16(4), 307–322, doi:10.1002/esp.3290160405, 1991.

Roering, J. J., Mackey, B. H., Handwerger, A. L., Booth, A. M., Schmidt, D. A., Bennett, G. L. and Cerovski-Darriau, C.: Beyond the angle of repose: A review and synthesis of landslide processes in response to rapid uplift, Eel River, Northern California, Geomorphology, 236, 109–131, doi:10.1016/j.geomorph.2015.02.013, 2015.

Scheingross, J. S., Minchew, B. M., Mackey, B. H., Simons, M., Lamb, M. P. and Hensley, S.: Fault-zone controls on the spatial distribution of slow-moving landslides, GSA Bull., 125(3–4), 473–489, doi:10.1130/B30719.1, 2013.

Schneider, J. M., Rickenmann, D., Turowski, J. M., Schmid, B. and Kirchner, J. W.: Bed load transport in a very steep mountain stream (Riedbach, Switzerland): Measurement and prediction: BED LOAD TRANSPORT RIEDBACH, Water Resour. Res., 52(12), 9522–9541, doi:10.1002/2016WR019308, 2016.

Schoenbohm, L. M., Whipple, K. X., Burchfiel, B. C. and Chen, L.: Geomorphic constraints on surface uplift, exhumation, and plateau growth in the Red River region, Yunnan Province, China, GSA Bull., 116(7–8), 895–909, doi:10.1130/B25364.1, 2004.

Schuerch, P., Densmore, A. L., McArdell, B. W. and Molnar, P.: The influence of landsliding on sediment supply and channel change in a steep mountain catchment, Geomorphology, 78(3), 222–235, doi:10.1016/j.geomorph.2006.01.025, 2006.

Shobe, C. M., Tucker, G. E. and Anderson, R. S.: Hillslope-derived blocks retard river incision, Geophys. Res. Lett., 43(10), 5070–5078, doi:10.1002/2016GL069262, 2016.

Simoni, A., Ponza, A., Picotti, V., Berti, M. and Dinelli, E.: Earthflow sediment production and Holocene sediment record in a large Apennine catchment, Geomorphology, 188, 42–53, doi:10.1016/j.geomorph.2012.12.006, 2013.

Sklar, L. S. and Dietrich, W. E.: Sediment and rock strength controls on river incision into bedrock, Geology, 29(12), 1087–1090, doi:10.1130/0091-7613(2001)029<1087:SARSCO>2.0.CO;2, 2001.

Sklar, L. S. and Dietrich, W. E.: A mechanistic model for river incision into bedrock by saltating bed load: BEDROCK INCISION BY SALTATING BED LOAD, Water Resour. Res., 40(6), doi:10.1029/2003WR002496, 2004.

Stolle, A., Schwanghart, W., Andermann, C., Bernhardt, A., Fort, M., Jansen, J. D., Wittmann, H., Merchel, S., Rugel, G., Adhikari, B. R. and Korup, O.: Protracted river response to medieval earthquakes, Earth Surf. Process. Landf., 44(1), 331–341, doi:10.1002/esp.4517, 2019.

Vulliet, L. and Hutter, K.: Viscous-type sliding laws for landslides, Can. Geotech. J., 25(3), 467–477, doi:10.1139/t88-052, 1988.

Wakabayashi, J.: Nappes, Tectonics of Oblique Plate Convergence, and Metamorphic Evolution Related to 140 Million Years of Continuous Subduction, Franciscan Complex, California, J. Geol., 100(1), 19–40, doi:10.1086/629569, 1992.

Whipple, K. X.: Bedrock Rivers and the Geomorphology of Active Orogens, Annu. Rev. Earth Planet. Sci., 32(1), 151–185, doi:10.1146/annurev.earth.32.101802.120356, 2004.

Wobus, C. W., Crosby, B. T. and Whipple, K. X.: Hanging valleys in fluvial systems: Controls on occurrence and implications for landscape evolution, J. Geophys. Res. Earth Surf., 111(F2), doi:10.1029/2005JF000406, 2006.

Wolman, M. G. and Miller, J. P.: Magnitude and Frequency of Forces in Geomorphic Processes, J. Geol., 68(1), 54–74, doi:10.1086/626637, 1960.

Yanites, B. J., Tucker, G. E., Mueller, K. J. and Chen, Y.-G.: How rivers react to large earthquakes: Evidence from central Taiwan, Geology, 38(7), 639–642, doi:10.1130/G30883.1, 2010.

Zhang, X., Phillips, C. and Marden, M.: Internal deformation of a fast-moving earthflow, Raukumara Peninsula, New Zealand, Geomorphology, 4(2), 145–154, doi:10.1016/0169-555X(91)90025-6, 1991.

Zimmermann, A., Church, M. and Hassan, M. A.: Step-pool stability: Testing the jammed state hypothesis, J. Geophys. Res. Earth Surf., 115(F2), doi:10.1029/2009JF001365, 2010.

Page 2: [1] Deleted **Noah Finnegan** **5/21/19 9:47:00 AM**

Page 6: [2] Deleted **Noah Finnegan** **5/21/19 9:47:00 AM**

Page 12: [3] Deleted **Noah Finnegan** **5/21/19 9:47:00 AM**

Page 12: [4] Deleted **Noah Finnegan** **5/21/19 9:47:00 AM**

Page 14: [5] Deleted **Noah Finnegan** **5/21/19 9:47:00 AM**

Page 15: [6] Deleted **Noah Finnegan** **5/21/19 9:47:00 AM**

		2-Year Mean Flow Depth (m)	Largest Field Measured Flow, Depth (m)	Channel Slope	2-Year Mean Bed Shear Stress (Pa)	Largest Field Measured Flow, Mean Bed Shear Stress (Pa)	2-Year Gravel Mobility Threshold (m)	Largest Field Measured Flow, Mobility Threshold (m)	Channel Width (m)

Page 15: [7] Formatted Table **Noah Finnegan** **5/21/19 9:47:00 AM**

Formatted Table

Page 15: [8] Deleted **Noah Finnegan** **5/21/19 9:47:00 AM**

Page 15: [9] Formatted **Noah Finnegan** **5/21/19 9:47:00 AM**

Font: Arial, 8 pt, Font color: Black, English (UK)

Page 15: [10] Formatted **Noah Finnegan** **5/21/19 9:47:00 AM**

Font: Arial, 8 pt

Page 15: [11] Formatted **Noah Finnegan** **5/21/19 9:47:00 AM**

Centered

Page 15: [12] Formatted **Noah Finnegan** **5/21/19 9:47:00 AM**

Font: Arial, 8 pt

Page 15: [13] Formatted **Noah Finnegan** **5/21/19 9:47:00 AM**

Centered

Page 15: [14] Formatted **Noah Finnegan** **5/21/19 9:47:00 AM**

Centered, Line spacing: single

Page 15: [15] Formatted **Noah Finnegan** **5/21/19 9:47:00 AM**

Font: Arial, 8 pt

Page 15: [17] Formatted **Noah Finnegan** **5/21/19 9:47:00 AM**

Centered

Page 15: [18] Formatted **Noah Finnegan** **5/21/19 9:47:00 AM**

Font: Arial, 8 pt, Font color: Black, English (UK)

Page 15: [18] Formatted **Noah Finnegan** **5/21/19 9:47:00 AM**

Font: Arial, 8 pt, Font color: Black, English (UK)

Page 15: [19] Formatted **Noah Finnegan** **5/21/19 9:47:00 AM**

Font: Arial, 8 pt

Page 15: [20] Formatted **Noah Finnegan** **5/21/19 9:47:00 AM**

Centered

Page 15: [21] Formatted **Noah Finnegan** **5/21/19 9:47:00 AM**

Font: Arial, 8 pt

Page 15: [22] Formatted **Noah Finnegan** **5/21/19 9:47:00 AM**

Centered, Line spacing: single

Page 15: [23] Inserted Cells **Noah Finnegan** **5/21/19 9:47:00 AM**

Inserted Cells

Page 15: [24] Inserted Cells **Noah Finnegan** **5/21/19 9:47:00 AM**

Inserted Cells

Page 15: [25] Inserted Cells **Noah Finnegan** **5/21/19 9:47:00 AM**

Inserted Cells

Page 15: [26] Formatted **Noah Finnegan** **5/21/19 9:47:00 AM**

Font: Arial, 8 pt

Page 15: [27] Formatted **Noah Finnegan** **5/21/19 9:47:00 AM**

Font: Arial, 8 pt

Page 15: [28] Formatted **Noah Finnegan** **5/21/19 9:47:00 AM**

Font: Arial, 8 pt

Page 15: [29] Formatted **Noah Finnegan** **5/21/19 9:47:00 AM**

Font: Arial, 8 pt

Page 15: [30] Formatted **Noah Finnegan** **5/21/19 9:47:00 AM**

Font: Arial, 8 pt

Page 15: [32] Formatted **Noah Finnegan** **5/21/19 9:47:00 AM**

Font: Arial, 8 pt

Page 15: [33] Formatted **Noah Finnegan** **5/21/19 9:47:00 AM**

Font: Arial, 8 pt

Page 25: [34] Deleted **Noah Finnegan** **5/21/19 9:47:00 AM**

Page 29: [35] Deleted **Noah Finnegan** **5/21/19 10:05:00 AM**